Spring 2004

Application of bootstrap resampling in fMRI

Arthika Bappal
New Jersey Institute of Technology

ABSTRACT

APPLICATION OF BOOTSTRAP RESAMPLING IN FMRI

by
Arthika Bappal

This thesis demonstrates the use of the bootstrap resampling technique considering temporal dependency in the fMRI data to determine the reliability and confidence interval of fMRI parameters. Traditionally, the test-retest method has been used to reliably detect active voxels in the fMRI image of the brain, which is based on repetitive experimentation. The main concern with the test-retest method is the reproducibility of data over these multiple repetitions. Fatigue, habituation, motion artifacts, and repositioning errors are few of the factors, which can affect the reproducibility of data.

The conventional bootstrap resampling technique is based on the assumption that the dataset is independent and identically distributed over time. However, studies have shown temporal dependency in the fMRI images of the brain acquired from subjects in the resting phase. This study demonstrates the use of the bootstrap resampling technique, incorporating the criterion of temporal dependency in the fMRI data set, to detect reliable active voxels in the fMRI images acquired during a task activated motor paradigm, where the subject is instructed to perform bilateral finger tapping.

The results of the study showed that the active regions detected using the bootstrap resampling technique considering temporal dependency in the fMRI data were more reliable than the active regions detected using the bootstrap resampling technique without considering any temporal dependency in the fMRI data.

APPLICATION OF BOOTSTRAP RESAMPLING IN FMRI

by
Arthika Bappal

A Thesis
Submitted to the Faculty of
New Jersey Institute of Technology
In Partial Fulfillment of the Requirements for the Degree of
Master of Science in Biomedical Engineering

Department of Biomedical Engineering

May 2004

APPROVAL PAGE

APPLICATION OF BOOTSTRAP RESAMPLING IN FMRI

Arthika Bappal

Dr. Stanley S. Reisman, Thesis Advisor — Date
Professor of Biomedical Engineering, NJIT
Professor of Electrical and Computer Engineering, NJIT

Dr Bharat B. Biswal, Co-Advisor — Date
Associate Professor of Radiology, UMDNJ

Dr. David Kristol, Committee Member — Date
Associate Chair and Professor of Biomedical Engineering, NJIT

BIOGRAPHICAL SKETCH

Author: Arthika Bappal

Degree: Master of Science

Date: May 2004

Undergraduate and Graduate Education:

- Master of Science in Biomedical Engineering
  New Jersey Institute of Technology, Newark, NJ, 2003.

- Bachelor of Science in Biomedical Engineering
  Manipal Institute of Technology, Manipal, KA, India, 2002.

Major: Biomedical Engineering

This thesis is dedicated to my beloved family and friends.

ACKNOWLEDGEMENT

I would like to first thank my research co-advisor, Dr. Bharat B. Biswal for his unwavering guidance, encouragement and support that greatly enhanced my graduate school education at New Jersey Institute of Technology. His expertise in the field of medical image processing and his valuable suggestions made my research work extremely enjoyable and rewarding.

Special thanks to my thesis advisor, Dr. Stanley Reisman for his guidance and supervision during the research. Also, thanks to Dr. David Kristol for serving as member of the thesis committee.

I am grateful to Radiology Department, University of Medicine and Dentistry of New Jersey for providing me the necessary infrastructure and support to carry out the research work.

I would also like to express my gratitude to everyone who directly or indirectly helped me during the course of the thesis. This thesis is dedicated to my family for whom I would like to express my love and gratitude.

TABLE OF CONTENTS

TABLE OF CONTENTS
(Continued)

Chapter **Page**

TABLE OF CONTENTS
(Continued)

Chapter **Page**

LIST OF TABLES

LIST OF TABLES
(Continued)

Table **Page**

LIST OF FIGURES

LIST OF FIGURES
(Continued)

Figure **Page**

LIST OF FIGURES
(Continued)

Figure **Page**

LIST OF FIGURES
(Continued)

Figure **Page**

CHAPTER 1

INTRODUCTION

1.1 Overview

Traditionally, for physiological and anatomical studies, neuroscientists have relied on animal models and human patients with localized brain damages to reveal the brain mechanisms of mental functions. Modern imaging techniques permits observe non-invasively, the neural activity of both normal and diseased human brain. Among noninvasive measurement techniques, functional magnetic resonance imaging (fMRI) is growing rapidly because of its superior spatial resolution and complete non-invasiveness.

Functional Magnetic Resonance Imaging measures brain response for a given stimulus. The main advantages of fMRI is that it is noninvasive, has a greater temporal and spatial resolution allowing for event-based and trial-based experiments and does not require exposure to radioactive isotopes. Blood Oxygenation Dependent (BOLD) functional MRI is the most commonly utilized method to measure brain activation in motor, visual, auditory cortex and in the areas of higher cognitive functions like speech, word generation and working memory.

To detect active regions in the fMRI images of the brain, researchers [1, 2] have used methods like the t-test, f-test, ANOVA and cross correlation. During activation, the signal intensity increases by about 5% above the mean signal intensity and by about 1% during rest, making it difficult to detect the active regions. Moreover, the presence of noise factors in the fMRI signal adds to the challenge of identifying the active regions reliably. Noise in functional MRI arises from a variety of sources. In most MR imaging,

the standard sources of noise are thermal noise from the subject, reception coil, preamplifiers and other electronics, and quantization noise from the analog to digital conversion. Also, uncontrolled or spontaneous neural events represent yet another source of noise.

It is important to devise methods, which can generate a measure for assessing the reliability and accuracy of the statistical parameters like t-test, cross correlation and ANOVA. The test-retest method [3-9] has been used to reliably detect active voxels in the fMRI image of the brain, which is based on repetitive experimentation. The main concern with the test-retest method is the reproducibility of data over these multiple repetitions. Fatigue, habituation, motion artifacts and repositioning errors are few of the factors, which can affect the reproducibility of data. Moreover, it is not possible to conduct repetitive scans on trauma patients and children.

To overcome the drawbacks of the test retest technique, statistical resampling methodologies have been proposed. Recently, the jackknife [10] and bootstrap resampling technique [11] has been developed, which can be used as an alternative to the test-retest method in reliable detection of active regions in fMRI images of brains. The basic principle behind these resampling techniques is generating a large pseudo population of the dataset by repeatedly resampling the original dataset. The statistical parameter of interest like the mean or correlation coefficient is calculated for each resampled dataset, and finally the distribution of this approximated statistical parameter is analyzed to find its confidence interval (explained in detail in Chapter 4).

The bootstrap and jackknife resampling techniques are based on the assumption that the dataset is independent and identically distributed over time. However, studies [12-18] have shown temporal dependency in the fMRI images of the brain acquired from subjects in the resting phase.

1.2 Objective

This study demonstrates the use of the bootstrap resampling technique, incorporating the criterion of temporal correlation in the fMRI data set, to detect reliable active voxels in the fMRI images acquired during task activation. Temporal dependency in fMRI datasets for different TR (time of repetition) is analyzed and the hypothesis that active regions detected considering temporal dependency in fMRI data is more reliable than the active regions detected without considering temporal dependency is tested.

1.3 Background Research

The test-retest technique is a commonly used tool to detect reliable active regions of the brain. In this technique, the experiment is repeated several times to increase reliability of data. In fMRI, considerable research has been done using this technique in recent years [3-9]. Yetkin et al. [3] were the first to investigate the use of the test-retest technique to obtain reliable measures. They showed that for each subject, activation from the first and second repetition of an experiment for motor and cognitive task was located in the same region. A measure of precision called the mean reproducibility ratio was defined as being the ratio of number of pixels activated by two experiments of the same task to the pixels activated by either experiment. Their studies showed that for a motor task, the mean

reproducibility ratio was 0.54, 0.59 and 0.57 at threshold levels of 0.70, 0.60 and 0.50 respectively and for sensory task was 0.39, 0.45 and 0.57 at thresholds of 0.70, 0.60 and 0.50.

Rombouts et al. [4] investigated the inter-subject and intra-subject variability of an activated area in the visual cortex. In terms of the size and shape of activated areas, the study showed higher inter-subject variability compared to intra-subject variability. For intra-subject variability, the mean values for reproducibility ratio of size was 0.83 ± 0.16 and for location was 0.31 ± 0.11.

Following the study of Yetkin et al. [3] and Rombouts [4], researchers developed statistical methods used along with the test retest technique to increase the reliability of active pixels. To define and quantify the reliability of the test-retest technique, Genovese et al. [5] recently proposed the maximum likelihood (ML) method. This method was used to set thresholds for detecting activation and determining the number of images that can be used for an experiment. Further extending this study, Maitra et al. [6] incorporated spatial context into the estimation process extending the premise of maximum likelihood (ML) developed by Genovese et al. [5]. They claim that their methodology provided more conservative estimates of true positives when compared to those obtained by Genovese et al. [5].

All studies on the test-retest technique [3-9] are based on the underlying assumption that the imaging parameters are constant over multiple scans. This technique might be effective in analyzing a simple motor or visual task. For more complex tasks, this assumption will not be valid. For example, for a simple finger tapping experiment, the imaging parameters and the stimulus related parameters like the finger tapping rate

and the ON/OFF cycle timing must be identical for each scan. Any deviation from the specified finger tapping rate or the ON/OFF cycles in any of the scans would result in an erroneous conclusion. Moreover the reproducibility of fMRI data for each repetitive scan can be affected by attentional efforts, motion artifacts, repositioning errors, learning, habituation or fatigue. Further, for a number of cases involving children and trauma patients, it is not possible to repeat the study a number of times.

Carel et al. [19], and Loubinoux et al. [20], have shown the test-retest effects for between sessions using time effect comparison. The study revealed prevalence of habituation shown by decreased activity of the primary sensorimotor cortex and SMA and an increased activity of the ipsilateral cerebellar hemisphere. Ramsey at al. [21] showed reduced extent of cortical motor activated areas, when the experiments were separated by 10-30 min or 5 to 16 weeks.

1.4 Outline

In Chapter 2, the basics of MRI and fMRI are briefly discussed. Chapter 3 discusses the currently used techniques for registration and statistical analysis of fMRI images. Chapter 4 describes three resampling techniques, the jackknife resampling technique, the bootstrap resampling technique, and the extension of the bootstrap resampling technique called the block bootstrap resampling technique. Subjects, task paradigm and data analysis are explained in Chapter 5. In Chapters 6 and 7 the results and future work are discussed.

CHAPTER 2

MAGNETIC RESONANCE IMAGING

2.1 Introduction

The concept of Nuclear Magnetic Resonance (NMR) was first demonstrated by Purcell [23] and Bloch [24] in 1946. In 1973 Lauterbur [25] and Mansfield [26] used the principles of NMR to describe a technique for determining physical structure properties. Since then, Magnetic Resonance Imaging (MRI) has been used in many biomedical, chemical and engineering applications. In this chapter, the basic principles of magnetic resonance imaging and functional magnetic resonance imaging are explained.

2.2 The Physics of MRI

Magnetic Resonance Imaging (MRI) is a non invasive imaging technique used primarily in medical settings to generate high quality images for studying the inside of human body. Magnetic Resonance Imaging is based on the principles of Nuclear Magnetic Resonance (NMR). The principle of NMR is derived from the quantum mechanical property of nuclear spin. Nuclei with odd number of neutrons or protons, or both will have a net magnetic moment making it NMR active. Among the most commonly used nuclei are Hydrogen, Carbon, Fluorine, Sodium, and Phosphorous. For medical imaging applications, "proton" NMR (hydrogen nuclei), is most common due to its high concentration in the human body and its high sensitivity [27].

The proton nucleus has two intrinsic properties - a magnetic moment and spin. When a magnetic field is applied, a torque is wielded on the nucleus causing it to align itself in the direction of magnetic field. However, temperature and other perturbations disturb this alignment. Over time, these thermodynamic and magnetic forces arrive at an equilibrium state with a small excess of protons aligned with the magnetic field. The combined alignments of these protons result in net magnetic moments, thereby inducing its own magnetic field. The spin causes the nuclei to precess about the magnetic field axis at a characteristic frequency rather than aligning themselves with the field. The frequency of precession, f is linearly proportional to the strength of the magnetic field B_0, as shown by the Larmor equation below [27].

$$f = \gamma B_0 \quad \text{(Hz)} \tag{2.1}$$

Where, γ is a proportionality constant specific to the nuclear species.

The magnetic moments of each nucleus can be divided two components - a stationary (longitudinal) component and a rotating (transverse) component. While the longitudinal component is on average in line with the applied magnetic field, the transverse component rotates about it. Normally, the phases of the rotational component of each nucleus are random with respect to each other, and thus, the net rotational field equates to zero [27].

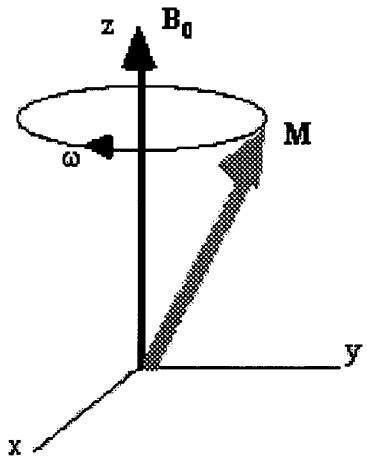

Figure 2.1 Precession of the magnetization vector in a static magnetic field aligned along the z-axis.

2.3 Image Contrast

The contrast in an MR image is strongly reliant on the image acquisition process. By adding RF or gradient pulses, and by careful choice of their timings, it is possible to highlight different components in the object being imaged. Contrast is generated by the varying degrees of spin density along the object, in the absence of which, there would be no NMR signal. Proton spin densities depend on water content, typical values of which are given in Table 2.1 for various human tissues [28]. The low proton spin density of bone makes MRI inappropriate for skeletal imaging. Since there is such a small difference in proton spin density between most other tissues in the body, other suitable contrast mechanisms must be employed. These are generally based on the variation in the values of T_1 and T_2 for different tissues.

Table 2.1 Water Content of Various Human Tissues

Tissue	%Water Content
Grey Matter	70.6
White Matter	84.3
Heart	80.3
Blood	93.0
Bone	12.2

T_1 Processes

At equilibrium, the net magnetization vector lies along the direction of the applied magnetic field B_o and is called the equilibrium magnetization M_o, shown in Figure 2.2. In this configuration, the Z component of magnetization M_Z equals M_o. M_Z is referred to as the longitudinal magnetization. There is no transverse (M_X or M_Y) magnetization here [27].

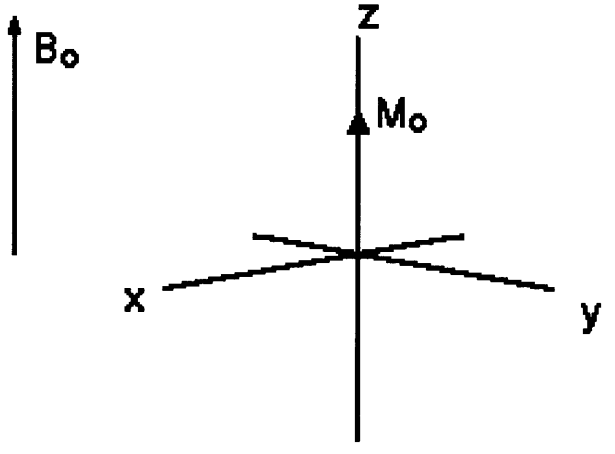

Figure 2.2 Longitudinal magnetization vector M_o in the direction of the magnetic field B_o.

It is possible to vary net magnetization by exposing the nuclear spin system to the energy of a frequency equal to the energy difference between the spin states. If enough energy is put into the system, it is possible to saturate the spin system and make

M_Z=0. The time constant, which describes how M_Z returns to its equilibrium value, is called the spin lattice relaxation time (T_1). The equation governing this behavior as a function of the time t after its displacement is:

$$M_z = M_o\,(1 - e^{-t/T_1}) \tag{2.2}$$

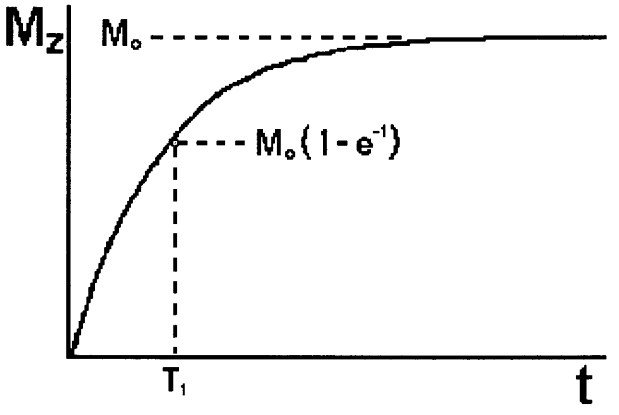

Figure 2.3 The T_1 relaxation curve.

The spin-lattice relaxation time T_1 is a measure of the time for the longitudinal magnetization to recover [27].

T_2 Processes

In addition to the rotation, the net magnetization starts to de-phase because each of the spin packets making it up is experiencing a slightly different magnetic field and rotates at its own Larmor frequency. The longer the elapsed time the greater the difference in phase. Here, the net magnetization vector is initially along XY, as shown in Figure 2.4. The time constant that describes the return to equilibrium of the transverse magnetization, M_{XY}, is called the spin-spin relaxation time, T_2 [27].

$$M_{XY} = M_{XYo}\, e^{-t/T2} \tag{2.3}$$

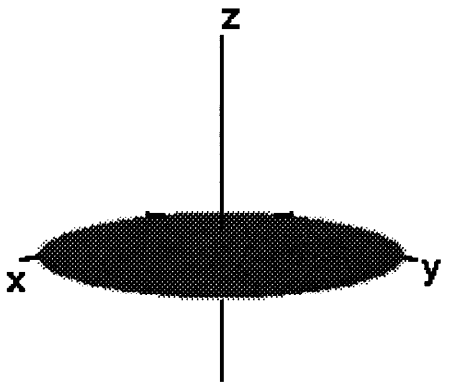

Figure 2.4 The net magnetization vector along the XY plane.

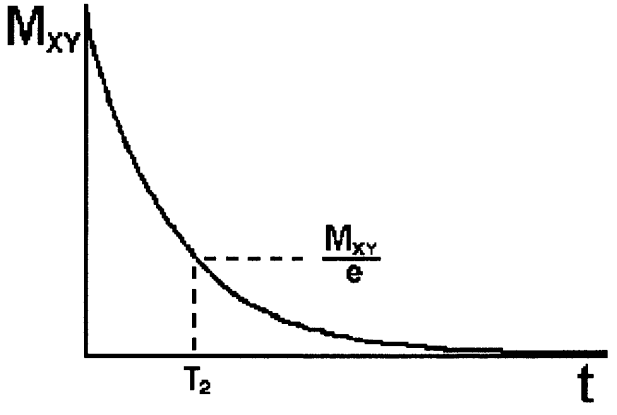

Figure 2.5 The T_2 relaxation cure.

The net magnetization in the XY plane goes to zero and the longitudinal magnetization grows until M_o is along Z. The transverse component rotates about the direction of applied magnetization and dephases [27]. The loss of transverse magnetization occurs relatively quickly whereas the return of excited magnetization to equilibrium takes a longer time.

Two factors contribute to the decay of transverse magnetization - Molecular interactions (said to lead to a pure T_2 molecular effect) and Variations in B_o (said to lead to an inhomogeneous T_2 effect). The combination of these two factors results in the decay of transverse magnetization. The combined time constant is called T_2 star and is given the

symbol T_2^*. The decay is exponential and is also called Free Induction Decay, FID. This rapid decay is due to the relationship between the T_2 from molecular processes and that from inhomogeneities in the magnetic field as follows.

$$1/T_2^* = 1/T_2 + 1/T_{2inhomo} \quad (2.4)$$

2.4 Magnetic Field Gradients

The measurement of frequency of precession of the magnetization in an NMR experiment, gives information on the field experienced by that group of spins. By manipulating the spatial variation of the field in specific ways, frequency information could yield spatial information. If each region of spin experienced a unique magnetic field their positions could be imaged. A gradient in the magnetic field is required to do this. A magnetic field gradient is a variation in the magnetic field with respect to position. A one-dimensional magnetic field gradient is a variation in only one direction, while a two-dimensional gradient is a variation in two. The more popular of the two gradients in magnetic resonance imaging is the one-dimensional linear magnetic field gradient. A one-dimensional magnetic field gradient along the x axis in a magnetic field, B_o, indicates that the magnetic field is increasing in the x direction. The symbols for a magnetic field gradient in the x, y, and z directions are G_x, G_y, and G_z [27].

2.4.1 Slice Selection Gradient

The RF pulses generated by RF antennas cannot spatially direct the RF energy. The slice selection gradient determines the slice of the tissue to be imaged in the body, in conjunction with the RF excitation pulse. For axial MR images, this gradient is applied along the long axis of the body, as shown in Figure 2.6. Proton precessional frequencies

vary according to their distance from the null of the slice selection gradient. A selective frequency RF pulse is applied to the whole volume, but only those spins along the gradient that have a precessional frequency equal to the frequency of the RF will absorb the energy due to the resonance phenomenon [29].

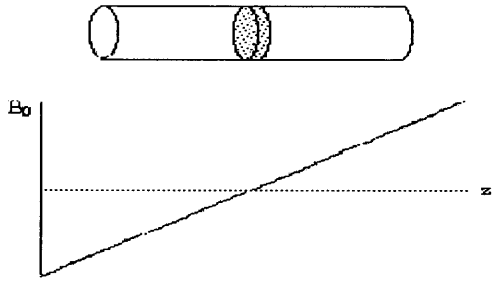

Figure 2.6 A long cylindrical object aligned along the z-axis in a field gradient which increases linearly with increasing z.

Slice thickness is determined by two parameters, (a) the bandwidth (BW) of the RF pulse, and (b) the gradient strength across the FOV. For a given gradient field strength, an applied RF pulse with a narrow BW excites the protons over a narrow slice of tissue, and a broad BW excites a thicker slice. For a fixed RF BW, the gradient slope determines the slice thickness. An increase in the gradient slope produces a large range of frequencies across the FOV and results in reduced slice thickness [29].

2.4.2 Frequency Encoding Gradient

The frequency encoding gradient, also known as the readout gradient, is applied in a direction perpendicular to the slice selection gradient. For an axial image acquisition, the frequency encoding gradient is applied along the x-axis throughout the formation and the decay of the signal arising from the spins excited by the slice selection gradient. Spins constituting the signal are frequency encoded, depending on their position along the

frequency encoding gradient. During the time the gradient is turned on, the protons precess with a frequency determined by their position from the null. Higher precessional frequencies occur at the positive pole and, lower frequencies occur at the negative pole of the gradient. Demodulation of the composite signal produces a net frequency variation that is symmetrically distributed from zero frequency at the center, to +fmax and –fmax at the edges of the FOV [29].

2.4.3 Phase Encoding Gradient

The position of the spins in the third spatial dimension is determined with a phase encoding gradient, applied before the frequency encoding gradient and after the slice selection gradient, along the third perpendicular axis. Phase represents the variation in the starting point of the sinusoidal wave, and can be purposefully introduced with application of a short duration gradient. After the initial localization of the excited protons in the slab of the tissue by slice selection gradient, all spins are in phase coherence. During the application of the phase encoding gradient, a linear variation in the precessional frequency of the excited spins occurs across the tissue slab along the direction of the gradient. After the gradient is switched off, spin precession reverts to the larmor frequency, but now phase shifts are introduced, the magnitude of which are dependent on the spatial position relative to the phase encoding gradient null and the strength. Phase advances for the protons in the positive gradients and phase retards for protons in the negative gradient, while no phase shifts occur for protons at the null [29].

To obtain T_1, T_2 or proton density weighted images, specific values of TR (time of repetition) and TE (time to echo) should be selected for a given pulse sequence. The selection of appropriate TR and TE weighs an image so that one contrast mechanism predominates the other two.

T_1 Weighted Image

A T_1-weighted spin echo sequence is designed to produce contrast based on the T_1 characteristics of tissues by de-emphasizing T_2 contributions. This is achieved with the use of a relatively short TR to maximize the differences in longitudinal magnetization during the return to equilibrium, and a short TE to minimize T_2 dependency during signal acquisition [29].

Proton Density Weighted Image

Image contrast with spin density weighting relies mainly on differences in the magnetizable protons per volume of tissue. At thermal equilibrium, those tissues with a greater spin density exhibit a larger longitudinal magnetization. To minimize the T_1 differences of the tissues, a relatively long TR is used. This allows a significant longitudinal recovery so that the transverse magnetization differences are mainly those resulting from variations in spin density. The influences of T_2 differences are minimized by using a short TE. Proton density weighted images therefore require a long TR and a short TE for the spin echo pulse sequence [29].

T_2 Weighted Image

A T_2-weighted spin echo sequence is designed to produce contrast based on the T_2 characteristics of tissues. This is achieved by reducing T_1 effects with long TR, and accentuates T_2 differences with a longer TE [29].

2.5 Pulse Sequence

The pulse sequence is a complex sequence of events, occurring during MRI data acquisition by switching on RF pulses and magnetic gradient fields. An MR pulse sequence comprises of three parts - the "preparation" or "excitation module", the "acquisition module" or "readout module" and a third "end module" which is used to modify or abolish remaining xy-plane magnetization prior to a succeeding spin excitation. All three modules are repeated multiple times to form an entire imaging pulse sequence during which the entire image points of the two-dimensional image or three-dimensional volume are measured.

In the following sections, four main pulse sequences used for MRI data acquisition are described briefly.

2.5.1 Spin Echo Pulse Sequence

The spin echo pulse sequence is the most commonly used pulse sequence. The pulse sequence timing can be adjusted to give T_1-weighted, proton or spin density, and T_2-weighted images. Dual echo and multi-echo sequences can be used to obtain both proton density and T_2-weighted images simultaneously. The two variables in spin echo sequences are the Time of Repetition (TR) and the Time of Echo (TE) [30].

All spin echo sequences include a slice selective 90 degree pulse followed by one or more 180 degree refocusing pulses as shown in the following diagram.

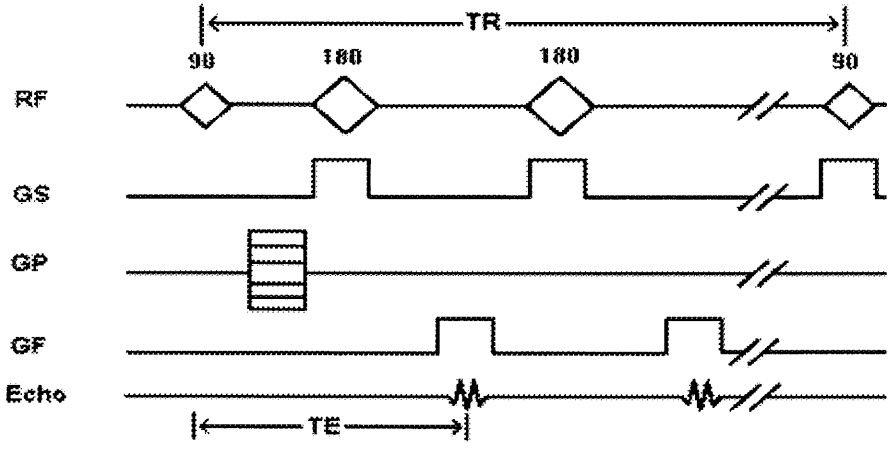

Figure 2.7 Timing diagram for spin echo pulse sequence.

2.5.2 Inversion Recovery Pulse Sequence

Inversion recovery pulse sequences are used to give heavy T_1-weighting. In addition, the STIR (Short T_1 Inversion Recovery) sequence can be used for fat suppression, where shorter inversion times are utilized to null the fat signal while maintaining water and soft tissue signal. The basic part of an inversion recovery sequence is a 180 degree RF pulse that inverts the magnetization. This is followed by a 90 degree RF pulse that makes the residual longitudinal magnetization into the x-y or transverse plane. This can now be detected by RF coils. In imaging, the signal is usually refocused with a 180 degree pulse as in a spin echo sequence. The time between the initial 180 degree pulse and the 90 degree pulse is the inversion time (TI) [30]. A diagram of the sequence is shown below.

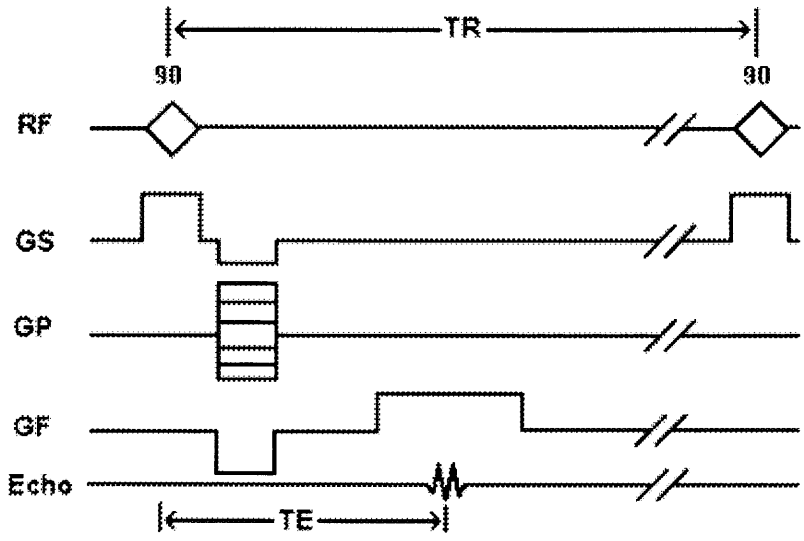

Figure 2.9 Timing diagram for Gradient Echo Pulse sequence.

2.5.4 Echo Planar Imaging

Echo planar imaging is a gradient echo technique related to fast gradient echo imaging. An entire set of 64 or 128 phase steps is acquired during one acquisition TR instead of one to 16 phase steps per acquisition TR. This is done by rapid reversal of readout or frequency- encoding gradient. This switching or reversal can also be done in a sinusoidal form. Echo planar sequences may use entirely gradient echos or may combine a spin echo with the train of gradient echos as illustrated in the diagram below. Echo planar images may be acquired in less that 1/10th of a second and therefore may be useful in cardiac imaging and other rapidly changing processes [30].

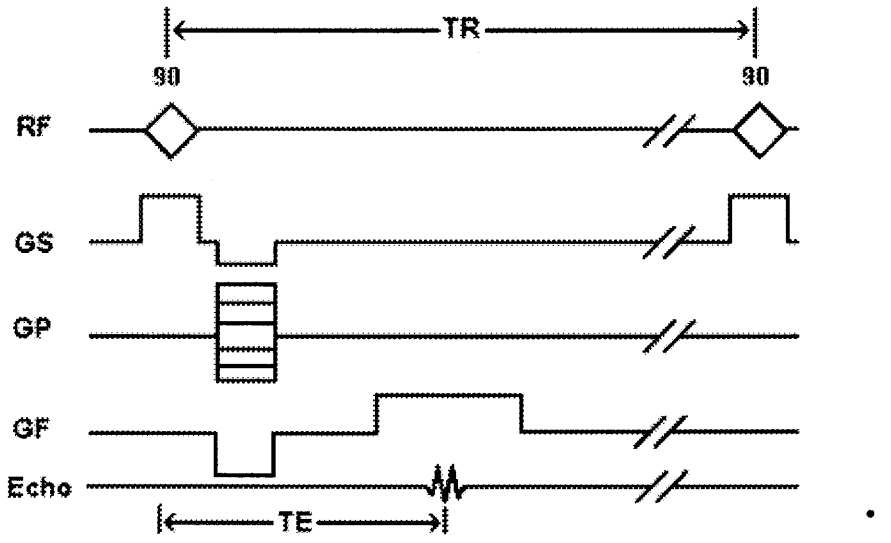

Figure 2.9 Timing diagram for Gradient Echo Pulse sequence.

2.5.5 Echo Planar Imaging

Echo planar imaging is a gradient echo technique related to fast gradient echo imaging. An entire set of 64 or 128 phase steps is acquired during one acquisition TR instead of one to 16 phase steps per acquisition TR. This is done by rapid reversal of readout or frequency- encoding gradient. This switching or reversal can also be done in a sinusoidal form. Echo planar sequences may use entirely gradient echos or may combine a spin echo with the train of gradient echos as illustrated in the diagram below. Echo planar images may be acquired in less that 1/10th of a second and therefore may be useful in cardiac imaging and other rapidly changing processes [30].

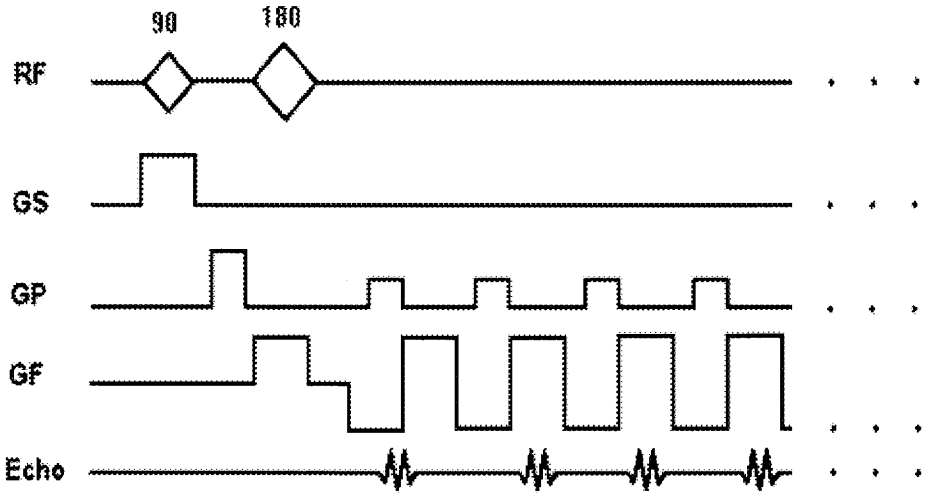

Figure 2.10 Timing diagram for spin Echoplanar Pulse sequence.

2.6 Functional Magnetic Resonance Imaging

Magnetic Resonance Imaging (MRI) of the brain is well-recognized for its excellent spatial resolution, allowing neuro-anatomic structures to be viewed in sharp detail. Recently, it has become possible to modify a conventional MRI scanner to study the brain's function as well. This new technology, called functional Magnetic Resonance Imaging (fMRI). Functional Magnetic Resonance is a non invasive technique used for measuring brain response to a given stimulus. There are four main types of functional MRI, (1) BOLD (Blood Oxygenation Dependent)-fMRI that senses variations in the blood oxygenation, (2) Perfusion fMRI which measures regional cerebral blood flow, (3) Diffusion-weighted fMRI which measures random movement of water molecules, and (4) CBV-fMRI, which measures variations in the cerebral blood volume. The signal to noise ratio obtained using BOLD method is high, compared to other methods. It is the most commonly used method to measure brain activation in motor, visual, auditory cortex and

in the areas of higher cognitive functions like speech, word generation and working memory.

2.6.1 BOLD Functional Magnetic Resonance Imaging

The BOLD method was introduced by Seiji Ogawa and his colleagues (1990) at the AT&T Bell laboratories [31]. Since regional blood flow is closely related to neural activity, measurement of the rCBF is useful in investigating brain function. The exact mechanism behind the BOLD contrast is still to be determined; however there is hypothesis which explains this mechanism.

The BOLD technique is based on the magnetic susceptibility of hemoglobin. Deoxygenated hemoglobin is paramagnetic, but when oxygenated, it becomes diamagnetic. The presence of the paramagnetic deoxy-hemoglobin distorts the static magnetic field. Spins in this non-uniform magnetic field now precess at different frequencies causing more rapid phase dispersal and decay of the NMR signal. Therefore, changes in blood oxygenation can cause changes in the MR decay parameter, T_2^*, leading to changes in image intensity in T_2^*-weighted images [32].

While neural activity increases the consumption of oxygen and the amount of deoxy-hemoglobin, the increase in blood flow that occurs a few seconds after the onset of activity results in a rapid influx of fresh, highly oxygenated hemoglobin into the capillaries and veins that far out weighs the prior decrease in oxygen. Consequently, the ratio of oxygenated to depleted hemoglobin increases during brain activation. As the ratio of oxy-hemoglobin to deoxy-hemoglobin increases, the rate (T_2^*) spin dephasing decreases due to fewer inhomogeneities that are caused by deoxy-hemoglobin. Finally,

this results in a brighter region in the functional MR image in areas of higher neural activity. [33]

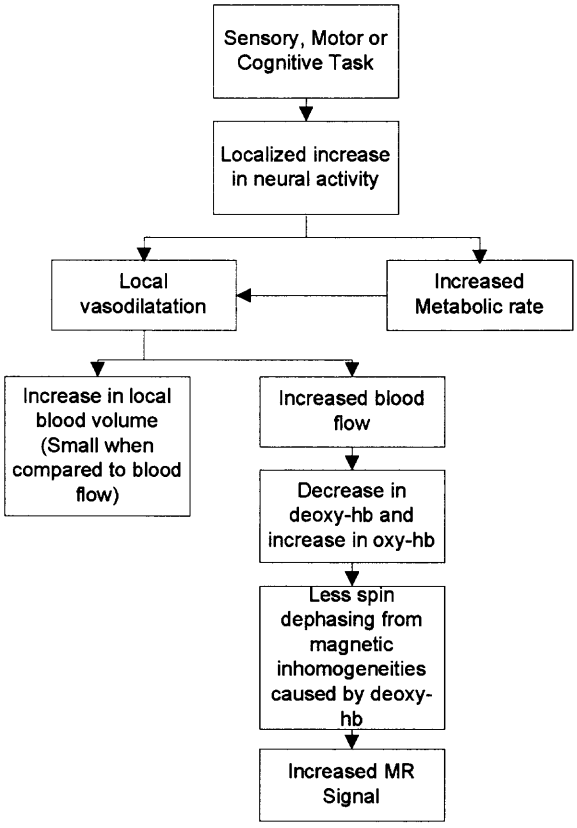

Figure 2.11 A hypothesized mechanism of changes in the blood oxygenation level dependent (BOLD) that underlie the FMRI approach to imaging task dependent neural activity.

Functional Mapping

To study brain function using fMRI, it is necessary to repeatedly image the brain, while the subject is presented with a stimulus or required to carry out some task. Most research is carried out using EPI since its fast acquisition rate enables detection of activation response to short stimuli and its reduced artifact from subject motion. The amount of T_2* weighting in the image is dependent on the echo time TE. If TE is too short, there will be

little difference in the T_2* curves for the activated state and the resting state, however if TE is too long then there will be no signal from either state. To obtain the maximum signal change for a region with a particular value of T_2*, the optimal value of echo time can be shown to be equal to the T_2* value of that tissue [35].

2.6.2 Paradigm Design

Designing the stimulus paradigm is as important as choosing the imaging parameters for a good experiment. The most common stimulus paradigm design is the blocked design, which has regular epochs of stimulus (active) and rest, as shown in Figure 2.12. The duration of the epochs should be long enough to accommodate the haemodynamic response, and so a value of at least 8 seconds, or more commonly 16 seconds should be chosen [35]. These epochs are repeated for as long as is necessary to gain enough contrast to noise to detect the activation response. The total experimental duration, however, must be a balance between how long the subject can comfortably lie still without moving, and the number of data points required to obtain enough contrast to noise. There are often some technical limitations to the experimental duration, and there is the possibility of the subject habituating to the stimulus causing the BOLD contrast to reduce with time [35]. Stimulus can also be presented in a random sequence, in which case, the pattern of the stimulus will not be known.

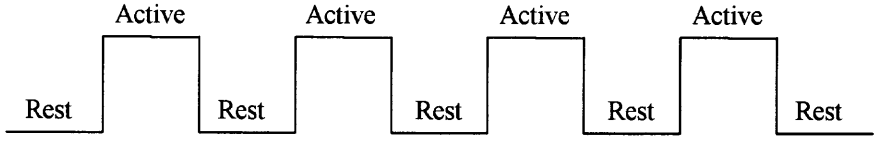

Figure 2.12 Representation of a box car reference waveform.

Event-Related design is another approach to present the stimulus. Unlike the traditional block design paradigm that strings identical event types together in a row, event-related fMRI allows for different event types to be interlinked in an arbitrary manner. Most importantly, while the block design is optimal for detecting activity in the brain, event-related fMRI is optimal for estimating the parameters of the hemodynamic response associated with individual events [36].

2.6.3 Noise Factors in fMRI

During scan, there are a number of physiological factors which induce noise. One factor, which affects the signal, is due to the cardiac and respiration cycle. Studies [12-18] have shown that rapid acquisition of echo planar images from subjects in the resting phase (during which no mental exercises are performed) comprise unstructured random noise in the MR signal together with cardiac (0.6-1.2 hz) and respiratory (0.1-0.5 hz) noise, and other oscillations below 0.1 Hz.

Another factor leading to artifact in fMRI is the signal coming from draining veins. Since gradient echo images are sensitive to vessels of diameters from micrometers to millimeters, it is difficult to distinguish between signals from the tissue and that from the veins, which could be some distance away from the activation site [37]. Also, the blood flowing into the imaging slice may be stimulus correlated. One way to reduce the signal from large vessels would be to use a spin echo sequence. This is sensitive to T_2 effects only and eliminates the dephasing effects from the large vessels [38, 39]. It is better to acquire a separate set of images which are sensitive to large vessels, and base this to decide the quality of signal [35].

Summary

This chapter discussed the basic principles involved in Magnetic Resonance Imaging and its extension to functional Magnetic Resonance Imaging. T_1 and T_2 contrast in MRI images can be used to differentiate varying tissue density levels in the brain, thereby obtaining a good contrast in the image. The Blood Oxygenation Level Dependent fMRI mechanism can be effectively used to measure the response of the brain to a stimulus. It is important to choose appropriate imaging parameters (RF pulse, TR, TE) and an effective stimulus paradigm to obtain a good fMRI image. The presence of noise factors during the scan presents a challenge to analyze the fMRI image and the following chapter discusses some of the methods to overcome the influence of noise factors.

CHAPTER 3

TECHNIQUES FOR fMRI DATA ANALYSIS

The method of analyzing fMRI data can be divided into three stages – preprocessing, statistical analysis and inference generation (shown in Figure 3.1). The raw data is preprocessed to improve the detection of activation events. This includes registering the images to correct for subject movement during the experiment and filtering the images to increase signal to noise ratio. Next, the preprocessed data is statistically analyzed to detect the image pixels, which show response to the stimulus. Finally, activation images are displayed and probability values computed to analyze statistical significance.

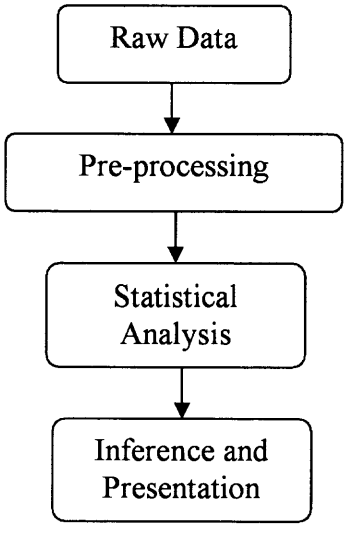

Figure 3.1 Steps involved in the processing of fMRI data.

3.1 Motion Correction

Motion correction is significant to accurately detect activations, as all subsequent analysis requires that each voxel correspond to a fixed location in the brain at every point in time. Subjects often tend to move in the scanner during the course of an experiment resulting in

motion artifacts. Therefore, all images need to be registered to a standardized coordinate system to enable further analysis. The motion artifacts can vary from small, sub-voxel motion to large, obvious motion. However, even sub-voxel motion result in detrimental effect on the statistical analysis — especially for smaller activations. Therefore, motion correction is required for almost all fMRI experiments.

In addition to rigid-body motion, sources of non-rigid motion like the pulsatile motion of the soft brain tissues during the cardiac cycle are also usually present. Even motions during respiration will change the magnetic field distribution throughout the body and will therefore affect the geometry of the scans. It is possible to reduce the extent of some of these motions by using methods such as cardiac gating of the images. However, the major component of motion is due to rigid movement of the head in the scanner, and it is the correction of this motion that is discussed in the following sections [40].

3.1.1 Woods' Automated Image Registration (AIR) Method

In 1992, Roger Woods et al. [41] developed a method for registration based on the assumption that if two images are accurately aligned, then the value of any voxel in one image is directly proportional to the value of the corresponding voxel in the other image. If the images are misaligned, the proportion is no longer constant but varies from voxel to voxel throughout the image. The registration algorithm systematically moves the test image relative to the reference image until this voxel-to-voxel variation is minimized.

Given two images u and v, let u denote the reference image and v the test image. First, the brain is segmented by thresholding in both images, based on the intensity levels of voxels. The voxel positions are denoted by i. If u(i) is the value of voxel i in image u

and v(i) is the value of the corresponding voxel in image v, let r(i) = u(i)/v(i) be the value of voxel i in the ratio image r. If r_{std} is the standard deviation of r and r_{mean} the mean value of r over all voxels, the algorithm uses the normalized standard deviation, r_{std} / r_{mean}, as a measure of how well the two images are aligned. To make the algorithm unbiased with regard to which image is designated the reference image, and which is designated the test image, the roles of the reference image and test image are switched. v is called the reference image, u is the test image and now u is transformed and a new normalized standard deviation, r'_{std}/r'_{mean}, is calculated. These two normalized standard deviations are then averaged to generate the R_{std}/R_{mean}, $R_{std} = (r_{std}+r'_{std})/2$ and $R_{mean} = (r_{mean}+r'_{mean})/2$. The algorithm minimizes R_{std}/R_{mean} by adjusting the transformation parameters, α and calculating R_{std}/R_{mean} iteratively [40].

3.1.2 Mutual Information Method

Mutual information (MI), or relative entropy, is a basic concept from information theory, measuring the statistical dependence between two random variables or the amount of information that one variable contains about the other. Collignon [41] and Viola and Wells [42] independently proposed the use of mutual information as a similarity measure in image registration, relating the joint entropy to the entropy of the two images, u and v separately [40].

The method is based on the assumption that MI measures the amount of information that image u contains about image v. Mutual information is derived from the entropy formulations of the images based on the frequency of observing a specific signal intensity in an image. This frequency is computed using probabilistic inference.

3.1.2 Least Square (LS) Measure

Hajnal et al. [44] presented a least-square similarity measure for intra modality registration of MR images and is used as registration technique for this thesis. Given two images u and v, the least square similarity is defined as

$$LS(u,v) = \sum_{i=1,j=1}^{N} \frac{(u_{(i,j)} - v_{(i,j)})^2}{N} \tag{3.1}$$

Where u (i,j) and v (i,j) denote signal intensity at voxel site (i,j) of image u and v, respectively, and N is the number of voxels in the overlapping region of the two images. This measure is fast to calculate, but can only be applied when the two images are of the same modality. The LS similarity measure is not applicable to multimodality registration results since the same tissue type has different intensity values in the two modalities. For example, bone appears bright in CT images but dark in MR images, so even though the images were perfectly aligned the LS function would evaluate to a rather large number. This is also true for registration of T_1-weighted and T_2-weighted MR images. Some benefits of this method are that it is easy to understand and implement and fast to evaluate [40].

3.2 Statistical Analysis of the Data

Many techniques have been proposed for statistically analyzing fMRI data to generate effective images identifying the regions that show significant signal change in response to the task.

3.2.1 Paired T-test

One of the simplest methods for obtaining results from an fMRI experiment is by simple subtraction. This is done by subtracting the averages of the images obtained during two different states of the stimulus. However, the presence of motion artifacts in the image can lead to inaccurate results using this technique. Also, this method does not generate a statistic to test against the null hypothesis. Hence, to obtain statistical significance, it is more common to use a Paired t-test [35].

The Paired T-Test quantifies the difference in means, by the standard deviation in the stimulus states, giving high t-scores to large differences with small standard deviations, and low t-scores to small differences with large standard deviations. The t-score is calculated on a pixel by pixel basis, for a time series X, using the Equation (3.2).

$$t = \frac{\overline{X}_1 - \overline{X}_2}{S_{\overline{X}_1 - \overline{X}_2}} \tag{3.2}$$

Where

$$S_{\overline{X}_1 - \overline{X}_2} = \sqrt{\frac{S_\gamma^2}{n_1} + \frac{S_\gamma^2}{n_2}} \tag{3.3}$$

Where

$$S_\gamma^2 = \frac{\sum (X_1 - \overline{X}_1)^2 + \sum (X_2 - \overline{X}_2)^2}{n_1 + n_2 - 2} \tag{3.3}$$

The suffix '1' refers to the $n1$ images acquired during the active period of the task, and '2' refers to the $n2$ images acquired during the rest period [35].

Often, there can be a delay in the hemodynamic response due to which, there is a shift in the response waveform. This delay needs to be incorporated while averaging the signal intensities of resting images.

T-test is generally used for simple, straightforward comparisons between two different states of stimulus. Since the T-values can be calculated by estimating the difference in the active and resting images, which are acquired separately, t-test is also applicable in situations where the stimulus sequence is unknown.

3.2.2 Correlation Technique

Since the BOLD response is mediated by blood flow, it is possible to improve the detection of activations by predicting the shape of the response to the stimulus, and calculating correlation coefficients between each pixel time course and their reference waveform. This is less sensitive to other physiological changes during the experiment, and to movement. For a time course X and a reference waveform Y, the correlation coefficient is calculated as,

$$r = \frac{\sum_{t=0}^{n-1}(X_t - \bar{X})(Y_t - \bar{Y})}{\sqrt{\sum(X_t - \bar{X})^2 \sum(Y_t - \bar{Y})^2}} \tag{3.5}$$

The equation estimates a value of 1 for perfect correlation, a value of zero for no correlation, and a value of -1 for perfect anti-correlation. The selection of an appropriate reference waveform is vital for the success of this technique in finding activations. Figure 3.2 represents a typical stimulus reference waveform and the signal below it corresponds to the response of the brain to the stimulus. The cross correlation of the two waveform shown in Figure 3.2 gave a correlation coefficient value of 0.73. Such a waveform does not account for the delay and smoothness of the haemodynamic response, which regulates the BOLD contrast. An improvement to this would be to change the phase of

the square wave, with the delay being between 3 and 6 seconds. To improve the reference waveform further, it is necessary to look more closely at the actual haemodynamic response. In an experiment, where there is both visual and motor activation, it is possible to use the response to one type of stimulus to form the reference waveform for finding the other. In this case, the time series for one or more pixels in, say the visual cortex is extracted, and correlation coefficients are calculated between this waveform and that of every other pixel in the image. Such an analysis detects only those regions in the brain, which respond to the stimulus in the same way as the visual cortex. The major disadvantage of this technique is that it is particularly sensitive to motion artifact, since if such artifact is present in the reference waveform then the movement of other regions will be highly correlated [35].

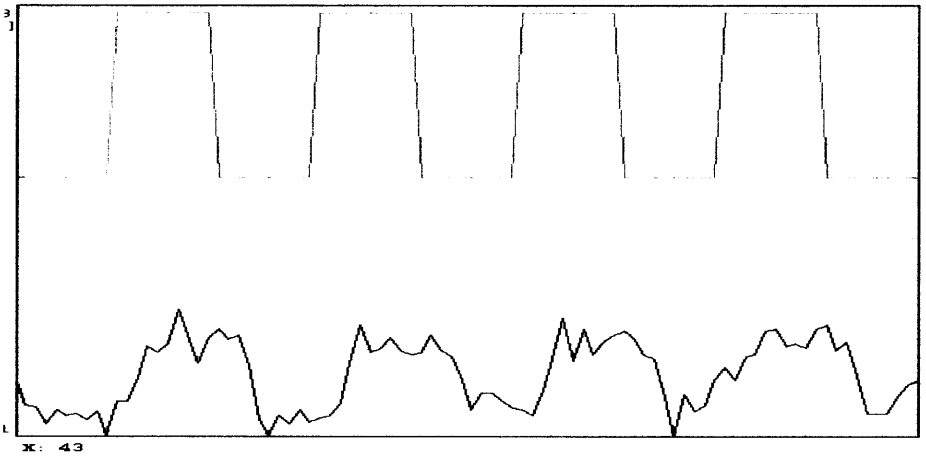

Figure 3.2 The waveform below represents the signal from an active voxel in the brain image in response to stimulus box car reference waveform shown above.

The distribution of correlation coefficient values between the ranges of –1 and +1, obtained by performing cross correlation between the reference waveform and each voxel in the resting image and active image is shown in Figure 3.3 (a) and (b). It is seen that for

a resting image, the distribution of the correlation coefficient is evenly spread between –1 and +1, with the mean almost close to zero and the distribution for the active image has correlation coefficient values greater than 0.4.

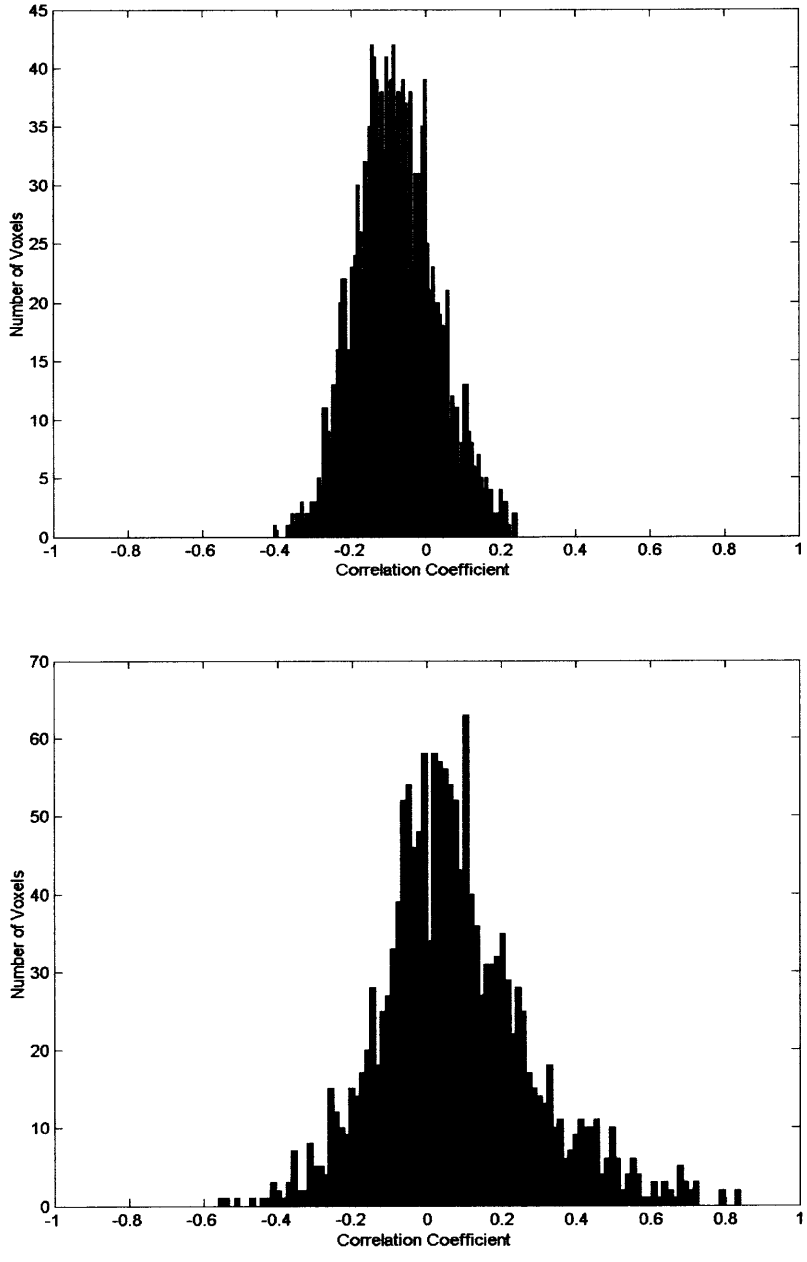

Figure 3.3 Distribution of the correlation coefficient values between the range of –1 and +1 for a resting image at the top (a) and for a active image (b) below.

To identify the active regions in this technique fixed threshold of correlation coefficient value is used. If the voxels had correlation coefficient values greater than the threshold value they are considered to be active. The problem with this method is that the same noise level and impulse response function is assumed for all the voxels, which might lead to less reliable detection of active regions.

The cross correlation technique can be used only when the stimulus reference sequence in know. The technique is easy to use and the significance level of the statistical parameter obtained is high because an assumption of the fMRI response timing and delay is used.

3.2.3 The General Linear Model

The statistical techniques described above assume that the observations are taken from normal populations and are special cases of the general linear model. The aim of the general linear model is to explain the variation of the time course $y1...yn$, in terms of a linear combination of explanatory variables and an error term. For a simple model with only one explanatory variable $x1...xn$, the general linear model can be written as,

$$y_i = x_u \beta + \varepsilon_i \tag{3.6}$$

Where β is the scaling, or slope parameter, and ε_i is the error term. If the model includes more variables it is convenient to write the general linear model in matrix form,

$$Y = X \beta + \varepsilon \tag{3.7}$$

Where now Y is the vector of observed pixel values, β is the vector of parameters and ε is the vector of error terms. The matrix X is known as the design matrix. It has one row for every time point in the original data, and one column for every explanatory

variable in the model. In analyzing an fMRI experiment, the columns of X contain vectors corresponding to the 'on' and 'off' elements of the stimulus presented. By finding the magnitude of the parameter in β corresponding to these vectors, the presence or absence of activation can be detected. β can be determined by solving the 'normal equations'

$$X^T Y = (X^T X)\hat{\beta} \tag{3.8}$$

Where $\hat{\beta}$ is the best linear estimate of β. Provided that $(X^T X)$ is invertible then is given by,

$$\hat{\beta} = (X^T X)^{-1} X^T Y \tag{3.9}$$

Such parameter estimates are normally distributed, and since the error term can be determined, statistical inference can be made as to whether the β parameter corresponding to the model of an activation response is significantly different from the null hypothesis [35].

For general linear model approach, it is necessary to know the pattern of the stimulus waveform. The general linear model can perform data analysis both within and between subjects and more than one reference waveform can be used to check for linear relationships between the response and reference waveforms.

3.2.4 Analysis of Variance (ANOVA)

This technique does not require any assumptions about the shape of the reference waveform and is based on simple signal averaging theory [45]. The time series contains two components, one is a genuine response to the signal, and the other is the random fluctuations due to uncorrelated physiological events and noise in the image. Upon averaging 32 cycles together, the magnitude of the noisy component is reduced but that

of the repeated signal is not. The reduction of the noisy component can be measured by calculating the variance of both the unaveraged and averaged data set.

To detect regions of activation, the ratio of the variance of the averaged data set to the variance of the unaveraged data set is calculated for each pixel in the image. For pixels in regions of purely random intensity variations, this ratio will be around $1/n$, where n is the number of cycles averaged together. Pixels in regions of activation, however, will have a significantly higher ratio than this, since the variance of both unaveraged and averaged data sets is dominated by the stimulus locked intensity variations of the BOLD effect, which does not reduce upon averaging.

If X_{ij} refers to pixel intensity measured at ith time point after the stimulus, of the jth trial of an experiment with n cycles and k points of interval per trail. The null hypothesis is that there is no significant difference in the means $\overline{X}_i$. This can be tested by comparing two estimates of the population variance, s_2, one based on variations in measurements of the same time point, and one based on the variance between time points.

The variance within measurement of any time point can be calculated by

$$s_i^2 = \sum_{j=1}^{n} \frac{(X_{ij} - \overline{X}_i)^2}{n-1} \tag{3.10}$$

and so the mean variance within time points is given by,

$$\hat{\sigma}_w^2 = \sum_{i=1}^{k} \frac{s_i^2}{k} \tag{3.11}$$

and is based on $k(n-1)$ degrees of freedom.

The variance of the time point means is given by,

$$s_{\bar{x}}^2 = \sum_{i=1}^{k} \frac{(\overline{X}_i - \overline{X})^2}{k-1} \tag{3.12}$$

$$\hat{\sigma}_B^2 = n \cdot s_{\bar{x}}^2 \tag{3.13}$$

Which is based on k-1 degrees of freedom. Under the null hypothesis, both $\hat{\sigma}_w^2$ and $\hat{\sigma}_B^2$ independently estimate the population variance s2. This means that the ratio

$$F = \frac{\hat{\sigma}_B^2}{\hat{\sigma}_w^2} \tag{3.14}$$

will have an F distribution with k-1 and $k(n$-1) degrees of freedom. If there is any signal change that is time locked to the stimulus, the value of will be larger than expected under the null hypothesis [35].

The ANOVA can be used in situations where the stimulus reference waveform is not known. ANOVAs are often used in the fMRI to make comparisons of signal activation within and across subjects.

Summary

This chapter provided an overview of the various steps involved in fMRI data analysis and a review of the various registration methods for motion correction like the Woods' Automated Image Registration technique, Mutual Information method and Least Square measure have been discussed.

The least square measure method, which is the image registration technique used in AFNI, has been adopted in this study to perform image registration. The chapter also discussed the various statistical methods for detecting the active voxels in an fMRI image. Methods like the paired T-Test, cross correlation and general linear model require

that the reference waveform be known. However, the application of ANOVA for statistical analysis does not require any assumptions of reference waveform and is based on simple signal averaging theory.

CHAPTER 4

RESAMPLING TECHNIQUES

The previous chapter discussed about the conventional statistical techniques like the paired t-test, cross correlation, and ANOVA to detect the active regions. These methods use a fixed threshold value for a statistical parameter to differentiate an active voxel from a non active voxel. The limitation with using a fixed threshold value is that same impulse response function and noise level is assumed for every voxel, which might lead to less reliable detection of active voxels.

Researchers have also used the test-retest method to reliably detect active voxels in the fMRI image of the brain. In the test-retest method the experiment is repeated several times and the data is statistically analyzed using methods like the t-test, cross correlation and ANOVA. The problem with this method is the reproducibility of the data over multiple repetition of the experiment. Fatigue and habituation due to repetitive experiments can alter the neuron firing rate affecting the reproducibility of the data. Moreover, motion artifacts and repositioning errors during repetitive experiments can also affect the reproducibility of data. Also, it is not possible to conduct repetitive scans on trauma patients and children.

To overcome the limitations of conventional methods the resampling technique has been developed. By performing resampling on a small original dataset, it is possible to generate a large pseudo population of the data, and thereby, avoid the need to repeat the experiment multiple times to obtain a large population of data.

To understand the basic principle of resampling, consider a sample $X = \{x_1, x_2, x_3 \ldots x_n\}$, the sample being a collection of independent identically distributed random variables of unknown distribution F. Let υ denote any statistical parameter of F, like the mean, variance, correlation coefficient or any other measure. The distribution of υ, forms the basis to obtain the confidence interval of υ. The distribution is obtained by repeatedly resampling from X and computing the new unknown characteristic, $\hat{\upsilon}$ for each of these resample. Thus, we obtain a distribution for $\hat{\upsilon}$ that approximates the actual distribution of υ, from which a confidence interval for υ can then be derived [46].

This chapter describes the various resampling techniques like jackknife, bootstrap and block bootstrap resampling used for estimating the reliability and confidence interval of the statistical parameters of interest.

4.1 Jackknife Resampling Technique

The jackknife resampling method was first developed by Maurice Quenouille and then used extensively by John Tukey for statistical analysis. In the Jackknife resampling technique the original data set is repeatedly resampled a large number of times by excluding a small number of data points, which is different every time the data is resampled. Thus, a large number of resampled data sets are obtained and the statistical parameter in question (mean, correlation coefficient) for each dataset is calculated. The distribution of a statistical parameter is then analyzed to obtain its confidence interval [10].

4.2 Bootstrap Resampling Technique

The bootstrap technique was first considered in a systematic manner by Efron in the year 1997. Bootstrap methodology is based on the theory of resampling. In the absence of any other knowledge, a good guide to the distribution in a population is the distribution of values found in a random sample of size n from the same population. The unknown real population is modeled from the infinite population which consists of n observed sample values, each with probability 1/n. The sampling is done with replacement, which makes bootstrapping different from randomization in many applications [49].

The general algorithm for the Bootstrap resampling technique is as follows:

1. Perform the experiment and obtain data $X = (x_1, x_2, x_3 \ldots x_N)$, which is independent and identically distributed.
2. Calculate the statistical parameter (mean, standard deviation or correlation coefficient) υ for the above data set.
3. Replicate each element of the above data set $(x_1, x_2, x_3 \ldots x_N)$ K times. K = 1000 was considered for this study.
4. The replicated data set is $X' = (x'_1, x'_2, x'_3 \ldots x'_{NxK})$.
5. Randomize the replicated dataset to obtain X''.
6. Create a new dataset $X^* = x_1^*, x_2^*, x_3^* \ldots x_N^*$ from the randomized dataset X''.
7. Calculate the statistical parameter in interest (mean, standard deviation or correlation coefficient) $\hat{\upsilon}$ for the above resampled data set X^*.
8. Repeat steps 5 to 7 a large number of times (was repeated 1000 times for this study).
9. Determine the confidence interval of υ using the distribution of $\hat{\upsilon}$.

The bootstrap resampling technique is similar to the jackknife resampling technique, the primary difference being that in jackknife, a minor fraction of data is neglected while resampling from the original data set. For small datasets, this might lead to a suboptimal estimation of statistical parameters. Moreover, the statistical significance is assumed to be the same for the resampled data set and the original dataset, which might also lead to erroneous detection of the active voxel. These limitations of the jackknife technique are overcome in the bootstrap resampling technique by keeping the size of the resampled data set the same as the original data set.

The bootstrap resampling technique is based on the assumption that each point in the data set is time independent. However, as explained in Chapter 2, Studies [12-18] have shown that rapid acquisition of echo planar images from subjects in the resting phase (during which no mental exercises are performed) comprise unstructured random noise in the MR signal together with cardiac (0.6-1.2 hz) and respiratory (0.1-0.5 hz) noise, and other oscillations below 0.1 Hz.

In the next section an extension of bootstrap resampling is explained, which incorporates the time dependency criterion in the dataset.

4.3 Block Bootstrap Resampling Technique

The block bootstrap resampling technique is an extension of the bootstrap resampling technique, which incorporates the criteria of temporal dependency in the data. Figure 4.1(a) and (b) shows the autocorrelation of two resting data sets. It is evident from the figure that the auto correlated values are non-zero positive integers, which signifies that the signal is not random and has some temporal dependency in it.

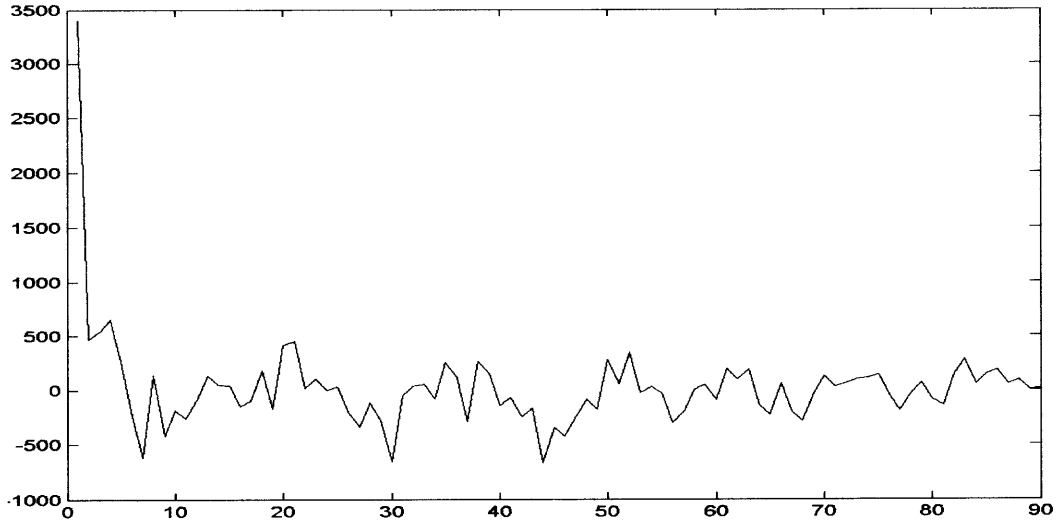

Figure 4.1(a) Represents the autocorrelation of a voxel from the resting data.

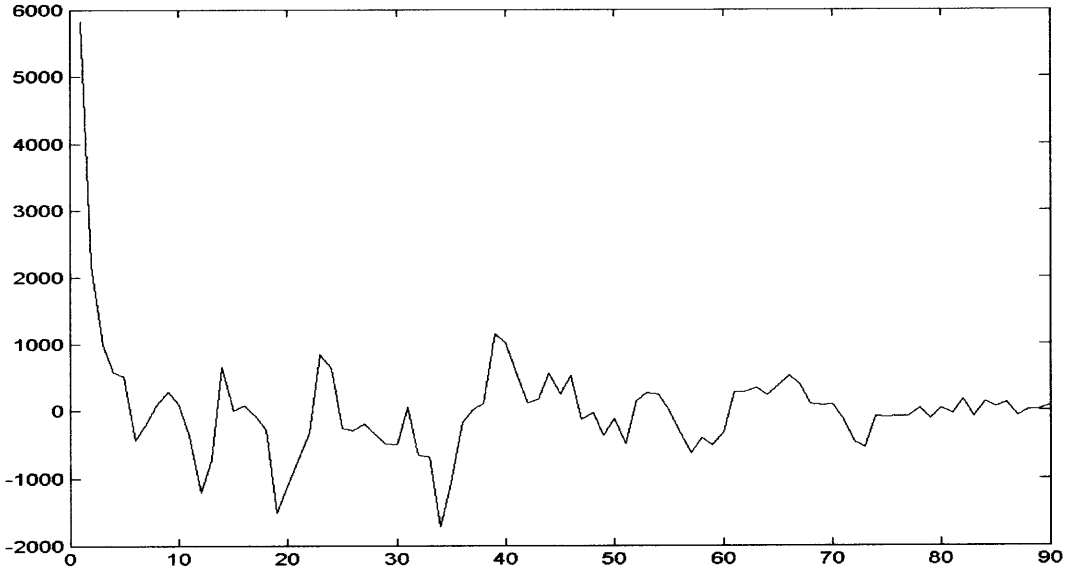

Figure 4.1(b) Represents the autocorrelation of another voxel from the resting data.

In the block bootstrap resampling technique, the dataset is divided into non overlapping blocks and the block size depends on the temporal dependency in the dataset. An example of the process of dividing data into blocks is illustrated below.

Consider a dataset X, which has N elements and data with block size D. Consider N = 20 and D = 5.

$X = [x_1\ x_2\ x_3\ x_4\ x_5\ x_6\ x_7\ x_8\ x_9\ x_{10}\ x_{11}\ x_{12}\ x_{13}\ x_{14}\ x_{15}\ x_{16}\ x_{17}\ x_{18}\ x_{19}\ x_{20}]$

This data is now divided into blocks of size 5 as shown below

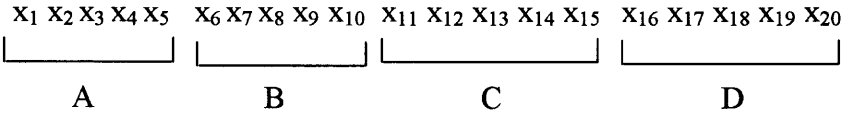

The maximum number of blocks that a data can be divided into is given by N/D. In block bootstrap resampling technique, the blocks are replicated multiple times, unlike in conventional bootstrap resampling where each element is replicated.

The general algorithm for the Bootstrap resampling technique is as follows:

1. Perform the experiment and obtain data $X = (x_1, x_2, x_3, .., x_N)$, which is independent and identically distributed.
2. Divide the original dataset into blocks of size D.
3. Replicate each block $(X_1, X_2, X_3 \ldots X_{(N/D)})$ K times. K = 1000 was considered for this study.
4. The replicated data set is $X'' = (X'_1, X'_2, X'_3 \ldots X'_{(N/D)xK})$.
5. Randomize the replicated dataset X''.
6. Create a new dataset $X^* = X_1^*, X_2^*, X_3^* \ldots X_N^*$ by selecting few blocks from the randomized dataset, until the number of points obtained combining the blocks equals the length of the original dataset.
7. Calculate the statistical parameter (mean, standard deviation or correlation coefficient) $\hat{\upsilon}$ for the above resampled data set.
8. Repeat steps 5 to 7 a large number of times (was repeated 1000 times for this study).
9. Determine the confidence interval of υ using the distribution of $\hat{\upsilon}$.

Hence, by using resampling techniques like the jackknife and bootstrap it is possible to generate a large pseudo population of data and thereby avoid the need to repeat the experiment multiple times to obtain a large data set. Using resampling techniques on an fMRI data set it is possible to generate the distribution of the statistical parameter for every voxel and use the mean and standard deviation of the distribution to determine its confidence interval. Hence, the noise level is considered for each voxel unlike the conventional fixed threshold method, which assumes the same noise level for each voxel in the image. This study is aimed to determine if better reliability of detecting active regions can be achieved by using the block bootstrap resampling technique incorporating the temporal dependency criterion in the fMRI dataset.

CHAPTER 5

EXPERIMENTAL METHODS AND DESIGN

To obtain a good quality fMRI image, it is essential to use high field MRI machine and choose the appropriate imaging parameters like the TR (Time of Repetition), and TE (Time to echo). It is also important to use stimulus paradigm design with suitable active and resting time period, which can produce a good signal response from the brain. Once the fMRI images are acquired the next step is to detect the regions in the brain that show a good response to the stimulus paradigm used. The signal from the brain increases only by 5% during activation and varies by 1% during rest and the presence of noise in fMRI signal, makes it difficult to identify activation. Hence it is essential to use the appropriate statistical technique to detect the active regions of the brain.

This study demonstrates the use of bootstrap resampling technique considering temporal dependency in the fMRI data set to determine the reliability and confidence interval for fMRI parameters. This chapter explains the process of implementing the bootstrap methodology on the fMRI data set and is also tested to see if better reliability in detecting active regions is achieved when compared to the conventional methods being used. This chapter also explains the data acquisition process and the design of the stimulus paradigm used.

5.1 Subjects and Data Acquisition

Seven healthy subjects, between 23 and 30 years of age (six male, one female) without any history of neurological illness volunteered for the fMRI scan. All subjects signed an informed consent approved by the Institutional Review Board of UMDNJ and each subject was paid on an hourly basis.

The subjects were made to lie straight inside a 3T Allegra Siemens MRI machine, with their head inside the birdcage head coil, as shown in Figure 5.1.

Figure 5.1 Picture of a patient lying in the MRI scanner.

A High resolution T1 weighted anatomical image was first obtained during scanning sessions. A gradient-recalled at steady state (GRASS) pulse sequence with TR = 600ms, TE = 10ms, FOV = 24cm and matrix size of 256x256 was used, resulting in a pixel resolution of 0.9375 mm×0.9375 mm×5 mm.

For functional images, five axial slices across the motor cortex were obtained using a gradient-recalled T_2* weighted echo planar imaging (EPI) pulse sequence. The fMRI scans were acquired using different TR (TR = 2000ms, TR=1000ms, TR = 500ms,

TR = 250ms), TE = 20 ms, FOV = 24 cm and a matrix size of 256x256 was used. This resulted in a pixel resolution of 0.9375mm×0.9375mm×5mm. For each TR, the resting fMRI scan was performed immediately after the task activated fMRI scan.

5.2 Task Paradigm

For this study, a motor task paradigm was used. Subjects were instructed to perform bilateral finger tapping for a set period of time, alternating with periods of rest. For this study fMRI images were acquired for two different sets of paradigm design. For the first set, fMRI images were acquired for different TR (time of repetition), TR = 2000 ms, TR = 1000 ms, TR = 500 ms, TR = 250 ms and for each TR the subjects were instructed to perform bilateral finger tapping for 20 secs, which is represented as ON, alternating with 20sec of rest, which is represented as OFF. The ideal box car reference waveform used for this experiment is shown in Figure 5.2.

For the second set, fMRI images were acquired for different TR, TR = 2000 ms, TR = 1000 ms, TR = 500 ms, TR = 250 ms, but the ON and OFF period during bilateral finger tapping varied for each TR. The ON and OFF period for, TR = 2000 ms, TR=1000ms, TR = 500 ms, TR = 250 ms, were 40ms, 20ms, 10ms, 5ms, respectively. The box car reference waveform used for acquiring this set of data is shown in Figure 5.3.

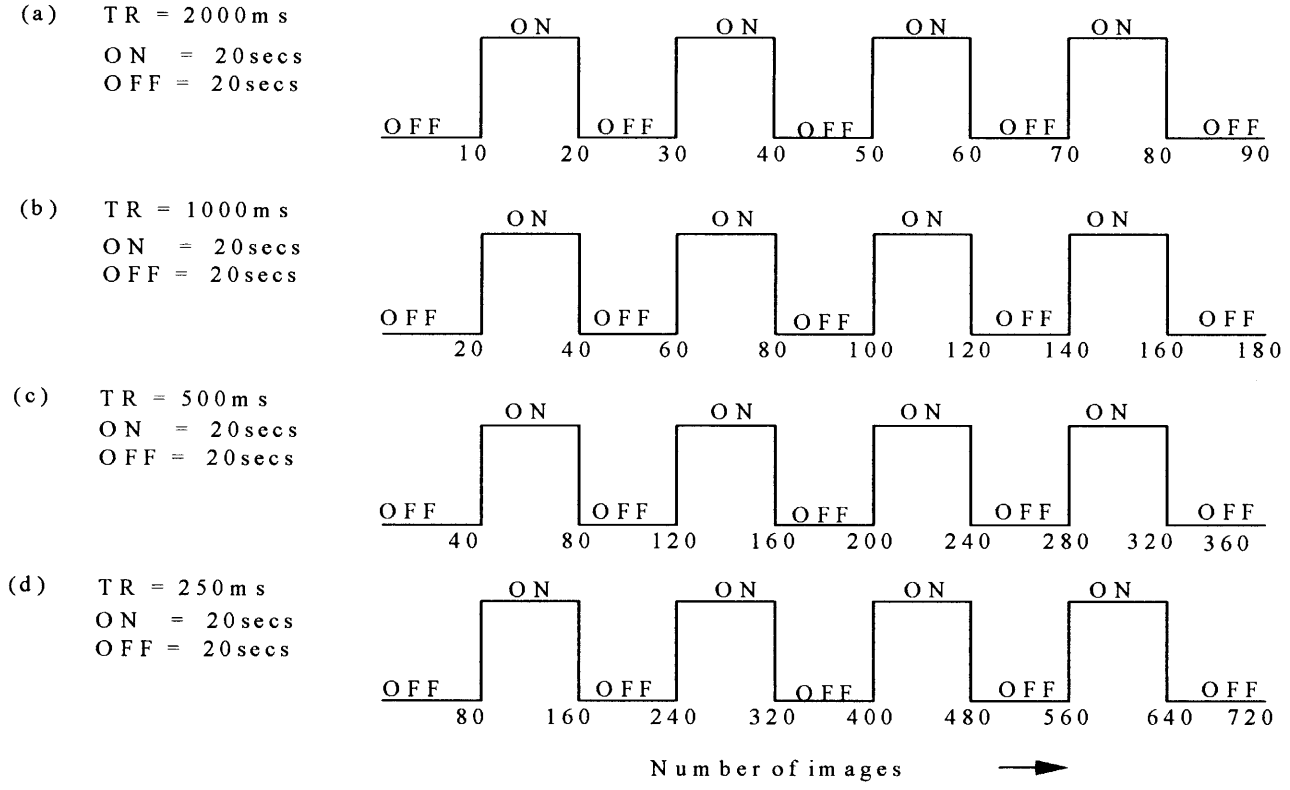

Figure 5.2 Representation of ideal box car reference waveforms used for acquiring the first set of data. Figure 5.2 (a),(b),(c),(d) are the reference waveform used for TR = 2000 ms, TR = 1000 ms, TR = 500 ms, TR = 250 ms with a (with 20 secs ON and OFF period) total of 90, 180, 360, 720 images acquired, respectively.

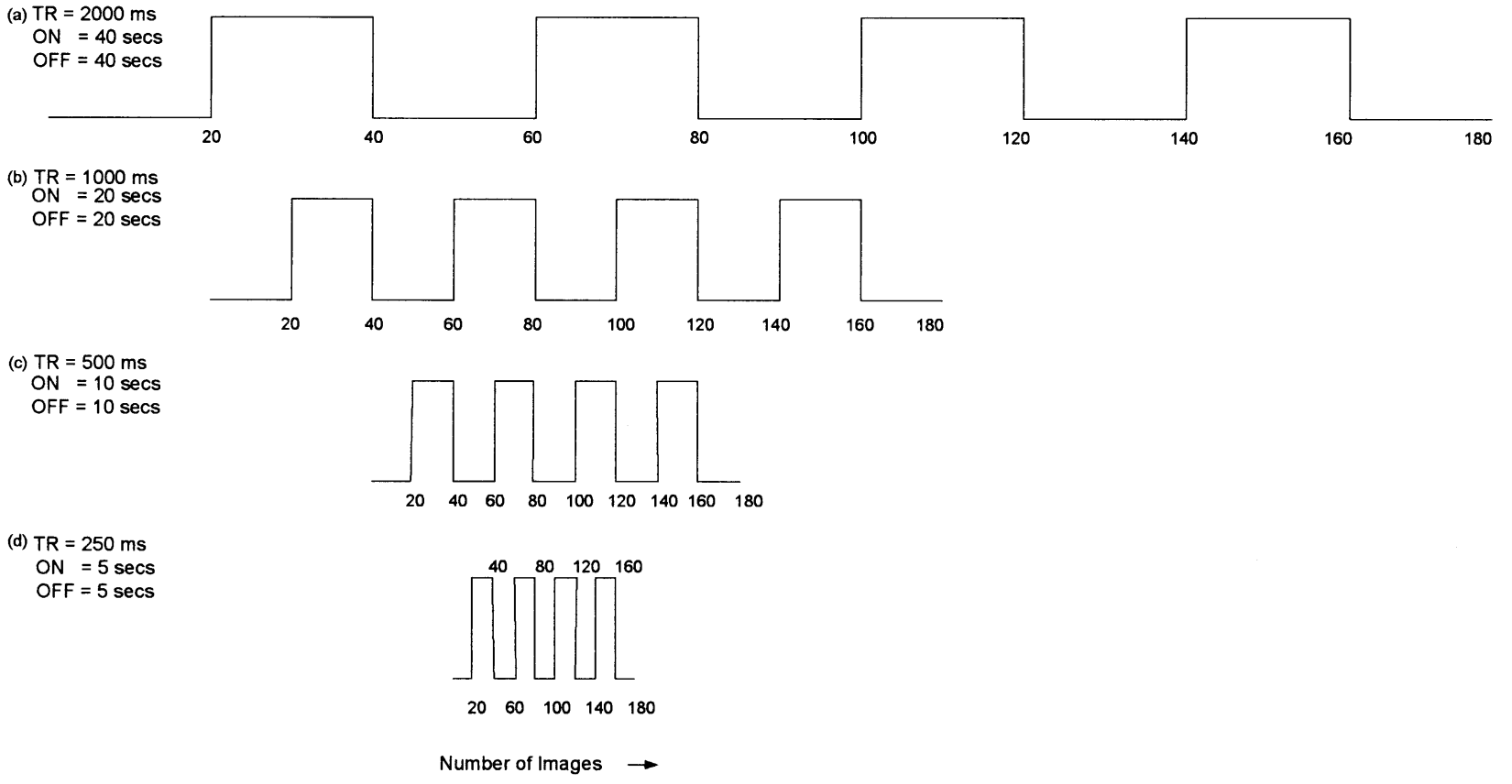

Figure 5.3 Representation of ideal box car reference waveforms used for acquiring the second set of data. Figure 5.3 (a),(b),(c),(d) are the reference waveform used for TR = 2000 ms, TR = 1000 ms, TR = 500 ms, TR = 250 ms (total of 180 images were acquired) with 40 secs, 20 secs, 10 secs, and 5 secs ON and OFF period, respectively.

5.3 Data analysis

The fMRI images were analyzed using AFNI software and one of the fMRI image acquired across the motor cortex of the brain during bilateral finger tapping is shown in Figure 5.3 (a) and its time series is shown in Figure 5.3 (b). Initially, the fMRI images obtained from each subject were passed through a registration algorithm using AFNI. The registration technique used is based on the least square method which is explained in Chapter 3.

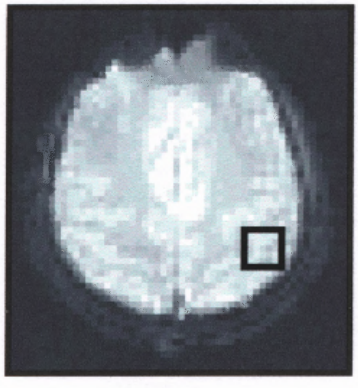

Figure 5.4 (a) An fMRI image acquired across the motor cortex of the brain during bilateral finger taping.

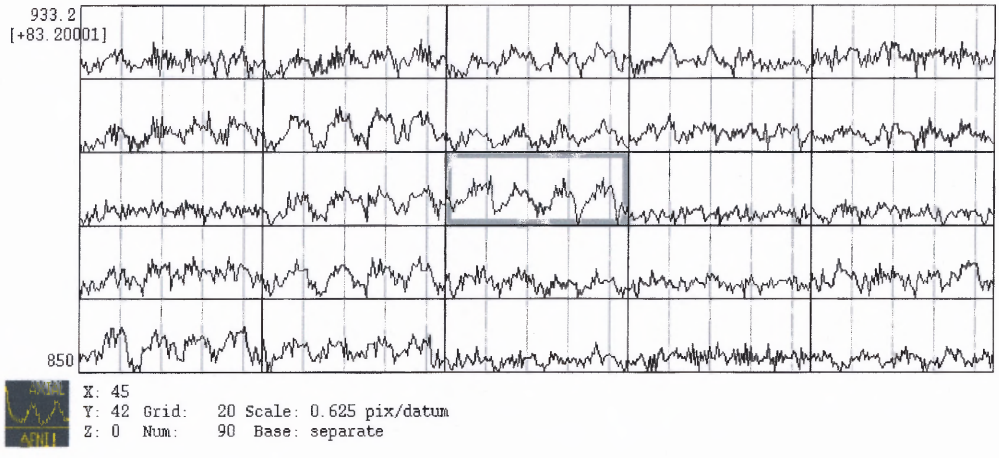

Figure 5.4 (b) The time series of the voxels shown in Figure 5.3(a).

5.3.1 Applying Bootstrap Resampling Technique

Neglecting the effect of temporal correlation, the bootstrap resampling technique was applied on all the active fMRI images obtained with different TR (TR = 2000 ms, TR = 1000 ms, TR = 500 ms, TR = 250 ms). Each point in the time series of the fMRI image and its corresponding point in the reference waveform were replicated 1000 times. To randomize the replicated data set, random numbers were generated and each random number was associated with a point in the replicated dataset and its corresponding point in the replicated reference waveform. The random numbers were arranged in ascending order, and from the randomized data set, the first few points were selected depending on the length of the time series of the fMRI image. Along with this, the corresponding reference points from the randomized data set were also selected. Next, cross correlation was performed between the chosen time points and the corresponding reference points. This process of randomizing and performing cross correlation was repeated 1000 times, resulting in 1000 correlation values for each voxel in the fMRI image. The process is depicted in the flowchart, shown in Figure 5.4.

The histogram for the 1000 correlation values for each voxel, generated using bootstrap resampling technique was calculated. Next, the mean and standard deviation of the 1000 correlation values for each voxel were obtained. The activation maps were generated that have the same confidence interval of the correlation coefficients at each voxel.

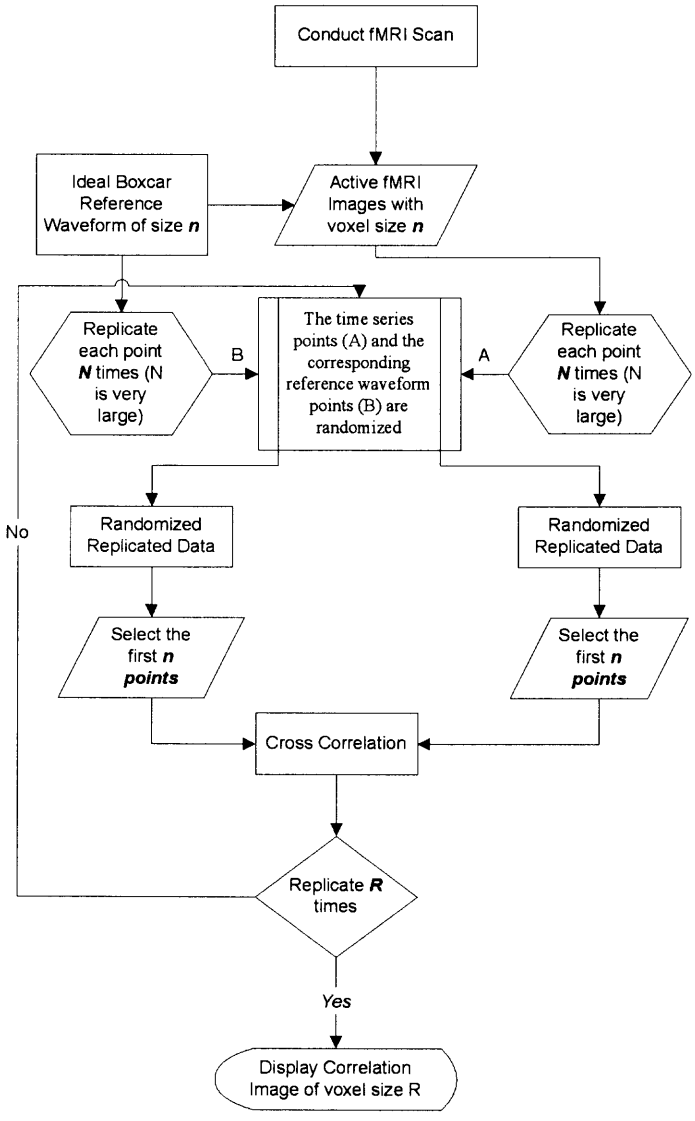

Figure 5.5 The flow chart for bootstrap resampling technique.

Table 5.1 Shows the Different Block Size Used for Each TR to Apply Block Bootstrap Resampling Technique

TR (Time of repetition)	2000 ms	1000 ms	500 ms	250 ms
Block Size	4,6,8,9,10,11, 12,14	14,16,18,19, 20,21,22,24	34,36,38,39, 40,41,42,44	74,76,78,79, 80,81,82,84

5.3.2 Applying Block Bootstrap Resampling Technique

Bootstrap resampling technique incorporating temporal dependency was applied on all the active fMRI images obtained using different TR. Here, the time series of each voxel in the fMRI image and its corresponding reference waveform was divided into equal sized blocks. The Block Bootstrap resampling technique was then applied on this data set. Each block in the time series and the corresponding block in the reference waveform were replicated 1000 times and randomized. From this randomized data set, a few time series blocks (sum of blocks equals the length of the time series) and its corresponding reference waveform blocks were selected. Next, the time series obtained by combining the blocks was cross correlated with the corresponding reference waveform obtained by combining the blocks. This entire process of randomizing the blocks and performing cross correlation was replicated 1000 times resulting in 1000 correlation values for each voxel. The flow chart for this method is shown in Figure 5.5. This method was repeated for different block sizes. Table 5.1 shows the block size that was used for fMRI image acquired using different TR (TR=2000ms, TR=1000 ms, TR=500ms, TR=250 ms). The mean, standard deviation and histogram of the 1000 cross correlation values for each voxel generated using different block size was then calculated. The mean correlation image generated using the bootstrap resampling technique (i.e. without considering temporal dependency in the fMRI data) was compared with the mean correlation image generated using different block size (i.e. considering temporal dependency in the fMRI data). The block size, which generated the image with highest correlation coefficient value, was considered as the block size for that TR. The activation maps were generated that have the same confidence interval of the correlation coefficients at each voxel.

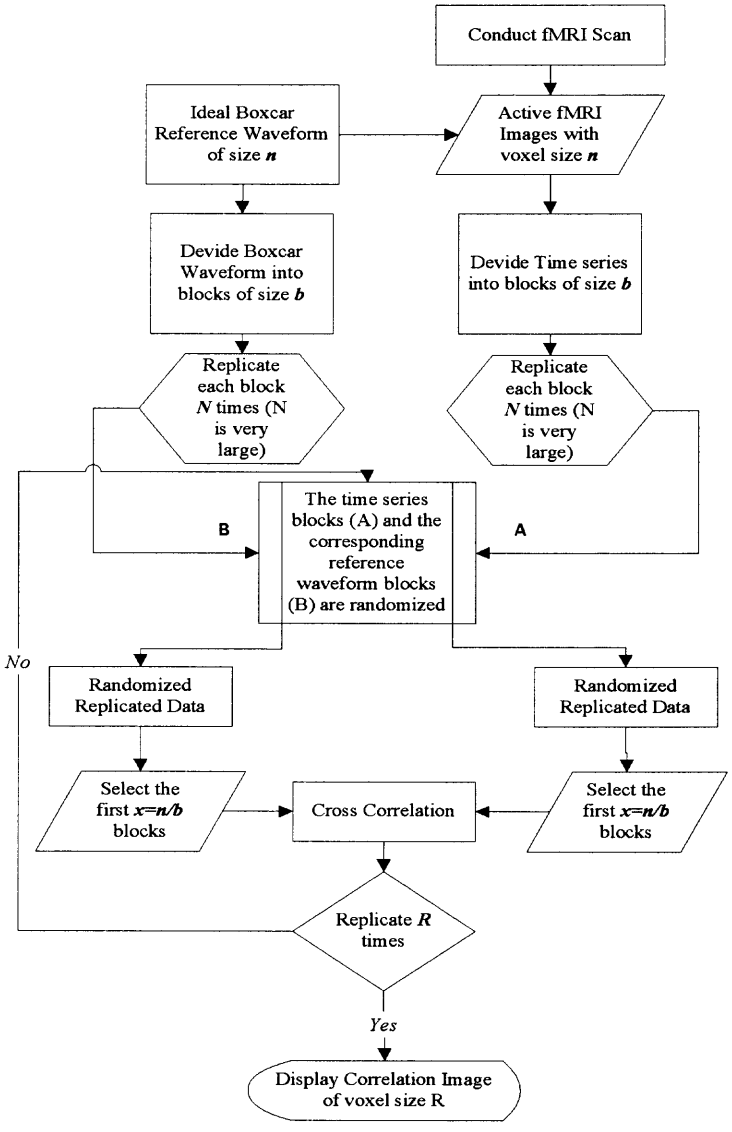

Figure 5.6 The flow chart for block bootstrap resampling technique.

5.3.3 Generating Activation Map Using Fixed Threshold

In order to compare the activation maps generated using the bootstrap and block bootstrap resampling technique, activation maps were generated using a fixed threshold of correlation coefficient in AFNI. The reference waveform was cross correlated with each voxel in the fMRI image and a fixed threshold of the correlation coefficient was used to determine the active voxels.

5.3.4 Applying T-test

The t-values were calculated instead of calculating the correlation coefficient for both bootstrap resampled data set and block bootstrap resampled data set. The purpose was to verify if a similar distribution for voxels were obtained using a different technique. For applying the t-test, the average of the signal intensity during activation was subtracted from the average of the signal intensity during rest. If the t-values obtained by subtracting were high then the voxel was considered to be active.

CHAPTER 6

RESULTS AND DISCUSSION

In this chapter, the results obtained using the fixed threshold of correlation coefficients, conventional bootstrap (without considering temporal dependency in the data) and block bootstrap resampling technique (considering temporal dependency in the fMRI data) was analyzed to observe the reliability in detecting the active voxels for each of these techniques.

6.1 Motion Correction

Subject head motion during the experiment is a main source of artifact in fMRI data. Hence, the first step in image analysis was to remove the motion artifacts due to head motion. The AFNI software, which uses the least-square based registration technique, was employed for correcting motion artifacts in fMRI images. Out of the seven subjects scanned, images from one subject were discarded due to the presence of motion artifacts even after image registration. To eliminate signal intensity variations arising from progressive saturation, the first four images of each time series from all the images were discarded.

6.2 Results Obtained Using Cross Correlation

The cross correlation images were obtained using the AFNI software. The stimulus reference waveform was cross correlated on a voxel by voxel basis with every voxel time course in the fMRI image. Figure 6.1 represents the histogram of the correlation

coefficient values, ranging from -1 to +1, obtained for every voxel in a resting fMRI image acquired using TR = 500 ms and Figure 6.2 represents the same for an active fMRI image acquired using TR = 500 ms. Observing the distributions in Figure 6.1 and 6.2, a correlation coefficient threshold of 0.4 was used to generate an activation map. Figure 6.3 represents the activation map obtained using a fixed threshold of 0.4 and displays activation in the motor cortex of the brain.

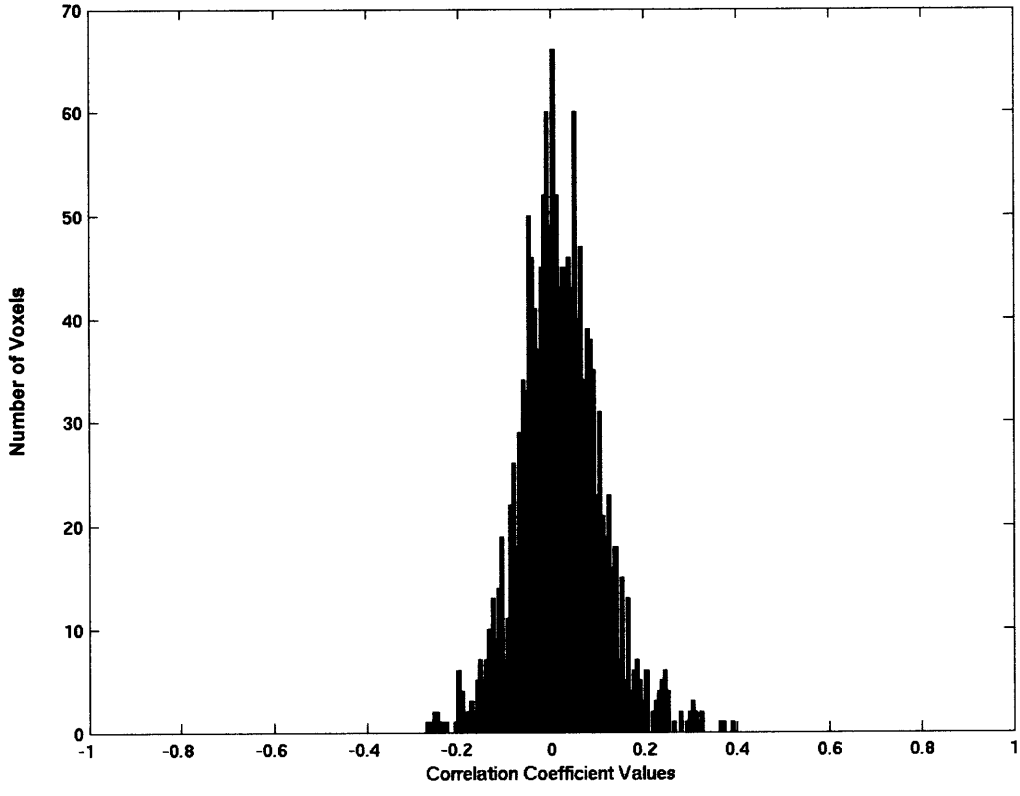

Figure 6.1 The histogram of the correlation coefficient values ranging from -1 to +1 obtained by cross correlating the stimulus reference waveform on a voxel by voxel basis with every time course in the resting fMRI image obtained using TR = 500 ms.

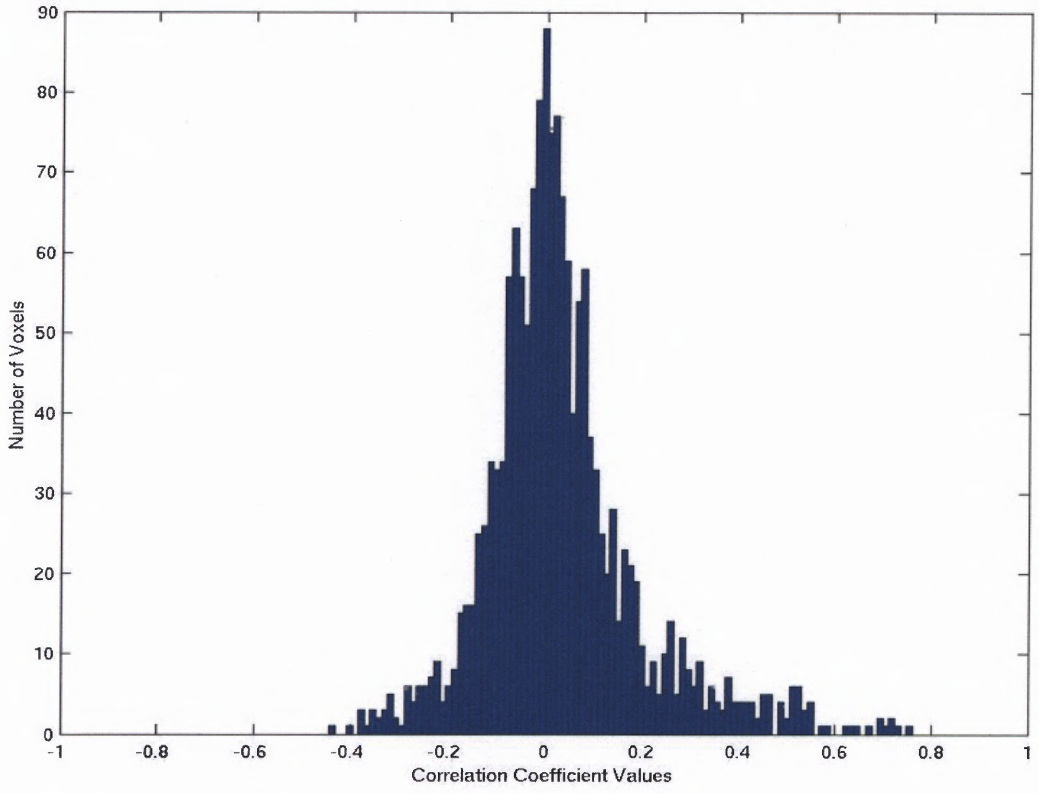

Figure 6.2 The histogram of the correlation coefficient values ranging from -1 to +1 obtained by cross correlating the stimulus reference waveform on a voxel by voxel basis with every time course in the active fMRI image obtained using TR = 500 ms.

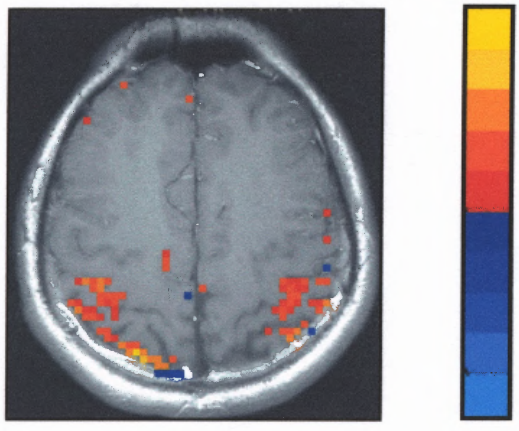

Figure 6.3 The activation map generated using a fixed threshold of 0.4 for the correlation coefficient values, for the fMRI image obtained using TR = 500ms.

The limitation of using a fixed threshold of correlation coefficient is that, the noise level is assumed to be same for all the voxels. This assumption might lead to less reliable detection of active voxels.

6.3 Results Obtained Using the Bootstrap Resampling Technique

The bootstrap resampling technique has been used in this study to estimate the reliability and confidence interval of the correlation coefficients for the fMRI image. In this method, each point in the time series and the corresponding reference waveform was replicated 1000 times and randomized. From the randomized data set, the first few time series points (equal to the length of the time series) and the corresponding reference waveform points were selected and cross correlated. This process of randomization and calculation of the correlation coefficients were repeated 1000 times. The bootstrap resampling technique generated 1000 correlation coefficients for each voxel in the image. The mean and standard deviation of 1000 correlation coefficients for each voxel were calculated. The cross correlation image obtained using the bootstrap resampling technique is shown Figure 6.4 (a). Figure 6.4 (b) represents the 1000 correlation coefficient values generated for the voxels shown in Figure 6.4 (a). Figure 6.4 (c) illustrates the histogram of the 1000 correlation coefficient values for the voxels shown in Figure 6.4 (a).

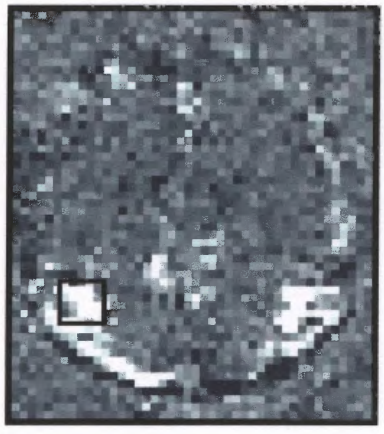

Figure 6.4 (a) Cross correlation image obtained applying the bootstrap resampling technique on fMRI image acquired using TR = 500 ms.

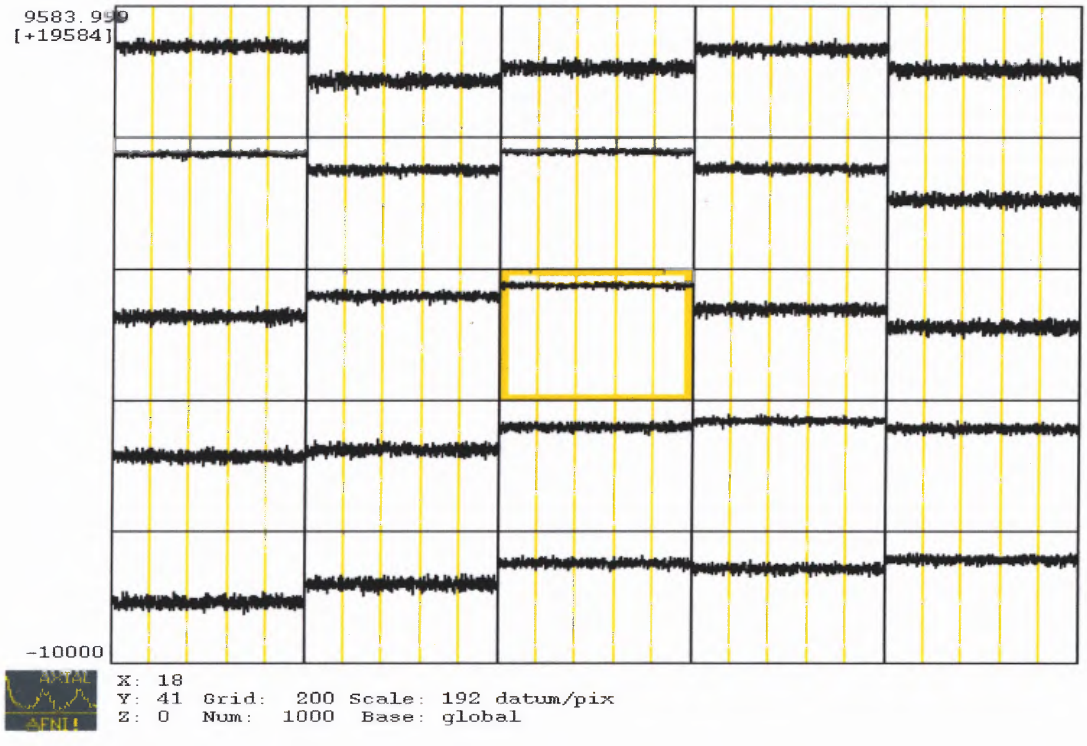

Figure 6.4 (b) Represents the 1000 Correlation coefficient values for the voxels shown in Figure 6.4 (a) generated using the bootstrap resampling technique.

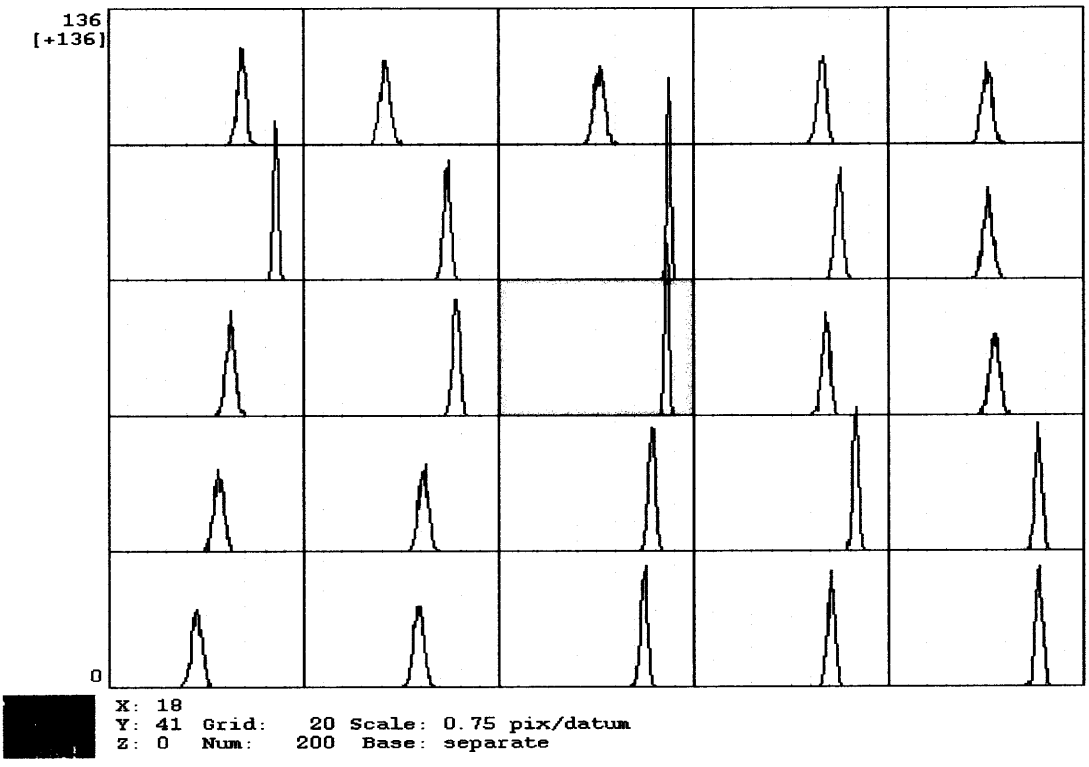

Figure 6.4 (c) The histogram of the correlation coefficient values ranging from -1 to +1 obtained using the bootstrap resampling technique for the voxels shown in Figure 6.4 (a).

The activation maps were generated by calculating the confidence interval of the correlation coefficient values for each voxel. Figure 6.5 (a) shows the activation map for the fMRI image obtained using TR = 500 ms, generated using a confidence interval of correlation coefficient mean greater than 8 times its standard deviation for each voxel. This indicates that voxels detected as active have a very high significance level. The activation maps generated using the bootstrap resampling technique (Figure 6.5 (a)) were compared with the activation map generated using a fixed threshold of 0.4 (Figure 6.5 (b)) for correlation coefficient value.

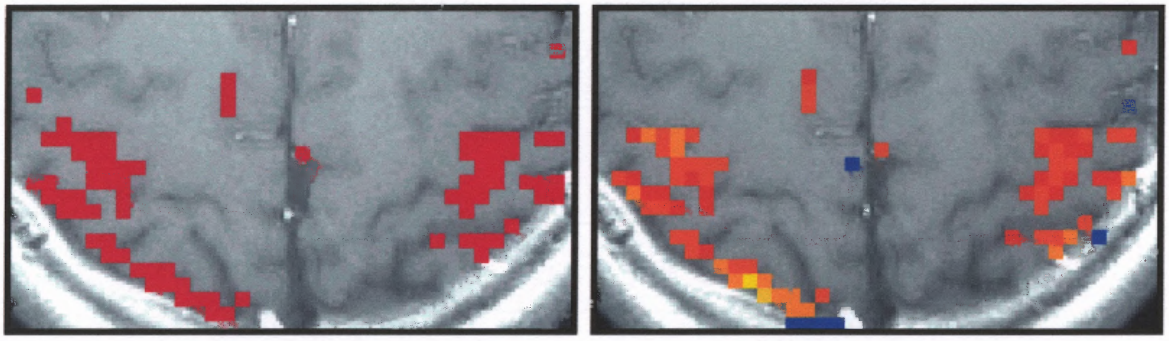

Figure 6.5 (a) and (b) shows the activation map generated using the bootstrap resampling technique and fixed threshold of correlation coefficient.

Observing the activation maps shown above, it can be seen that the activation map generated using the confidence interval of the correlation coefficient shows less extraneous voxels outside the motor cortex as active, when compared to the activation map generated using the fixed threshold of correlation coefficient value. Hence, a better reliability in detecting active regions can be achieved by generating the activation map using the distribution of the correlation coefficients for each voxel.

6.4 Results Obtained Using the Block Bootstrap Resampling Technique

The block bootstrap resampling technique is an extension of the conventional bootstrap, incorporating temporal dependency in fMRI dataset. In the block bootstrap, the time series and the corresponding reference waveform were divided into equal sized, non overlapping blocks. These blocks were then replicated and randomized, unlike the conventional bootstrap resampling technique, where each element in the time series was replicated (both the replicated time series and the corresponding reference waveform blocks are randomized in the same way). From this randomized dataset, the first few time series blocks (sum of blocks equals the length of the time series) and the

corresponding reference waveform blocks were chosen and cross correlated. This process of randomizing and calculating correlation coefficients was repeated 1000 times and the mean and standard deviation of 1000 correlation coefficients for each voxel were calculated.

The first step in analyzing the results for the block bootstrap technique was to observe if higher mean correlation coefficient values were obtained, by considering the block sizes shown in Table 6.1, when compared to the mean correlation coefficient values obtained by applying the conventional bootstrap. The mean correlation coefficient, obtained by using a block size, which gave maximum coerrelation coefficient, is considered as the block size for that particular TR.

Table 6.1 Shows the Different Block Size Used for Each TR to Apply Block Bootstrap Resampling Technique

TR (Time of repetition)	**2000 ms**	**1000 ms**	**500 ms**	**250 ms**
Block Size	4,6,8,9,10,11, 12,14	14,16,18,19, 20,21,22,24	34,36,38,39, 40,41,42,44	74,76,78,79, 80,81,82,84

Two cases have been illustrated to show the variation in correlation coefficient values obtained using block bootstrap. For the first case, fMRI image acquired using TR = 1000 ms and for the second case, TR = 500 ms was used as illustrated in Figure 6.6 and 6.7, respectively.

Figure 6.6 (for image with TR = 1000 ms) graphically compares the difference in mean correlation coefficients between block bootstrap (considering different block sizes) and conventional bootstrap resampling technique for voxels at the motor cortex. Each subplot illustrates the variation in mean correlation coefficient for 5 different block sizes-

14, 16, 18, 19 and 0. The block size zero essentially represents the conventional bootstrap resampling technique. It is evident from the plots that the mean correlation coefficients for block size 18 are high in most voxels.

Similarly, Figure 6.7 (image with TR = 500 ms) graphically compares the difference in mean correlation coefficients between the block bootstrap and conventional bootstrap resampling technique for voxels at the motor cortex. Each subplot illustrates the variation in mean correlation coefficient for 5 different block sizes- 34, 36, 38, 39 and 0. It is evident from the plots that the mean correlation coefficients for block size 36 are high in most voxels.

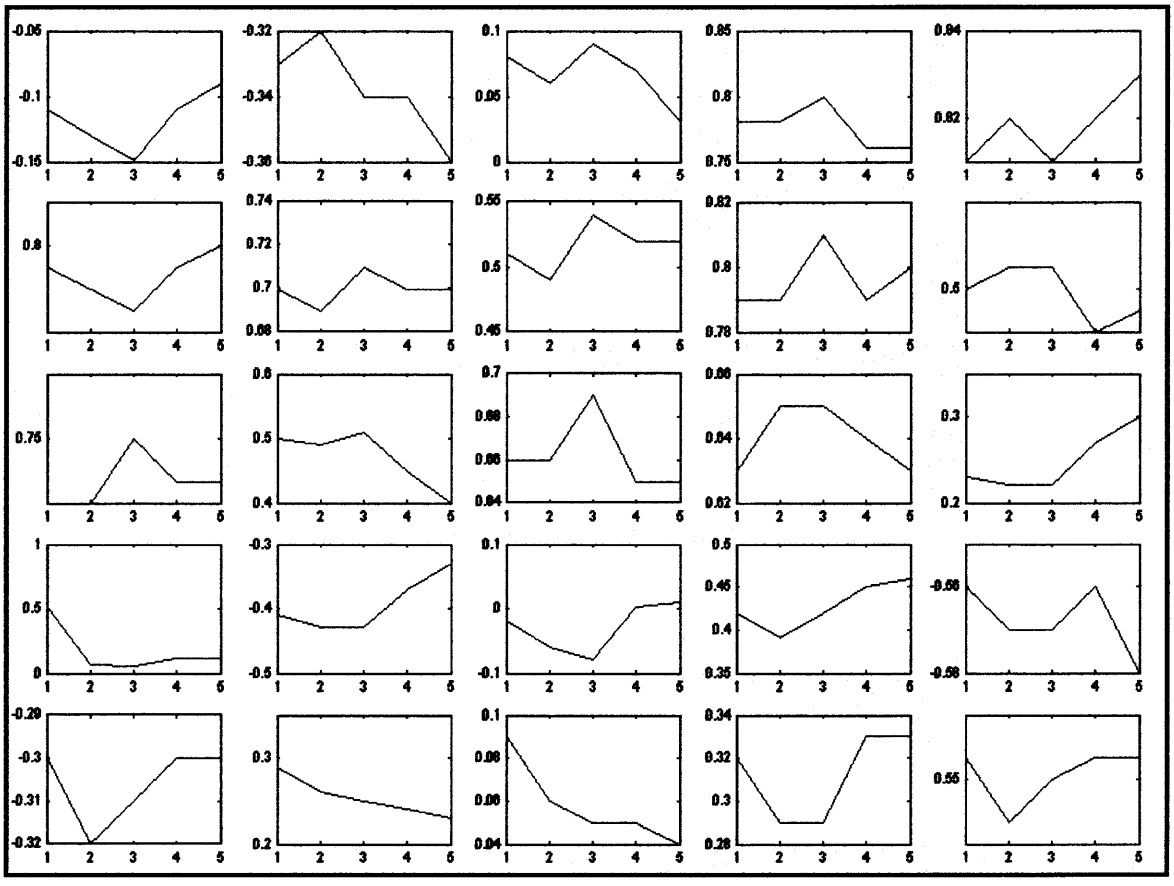

Figure 6.6 Represents subplots comparing mean correlation coefficient values obtained applying block bootstrap, with block sizes 14, 16, 18, 19 and 0 (conventional bootstrap resampling technique) for voxels in the motor cortex.

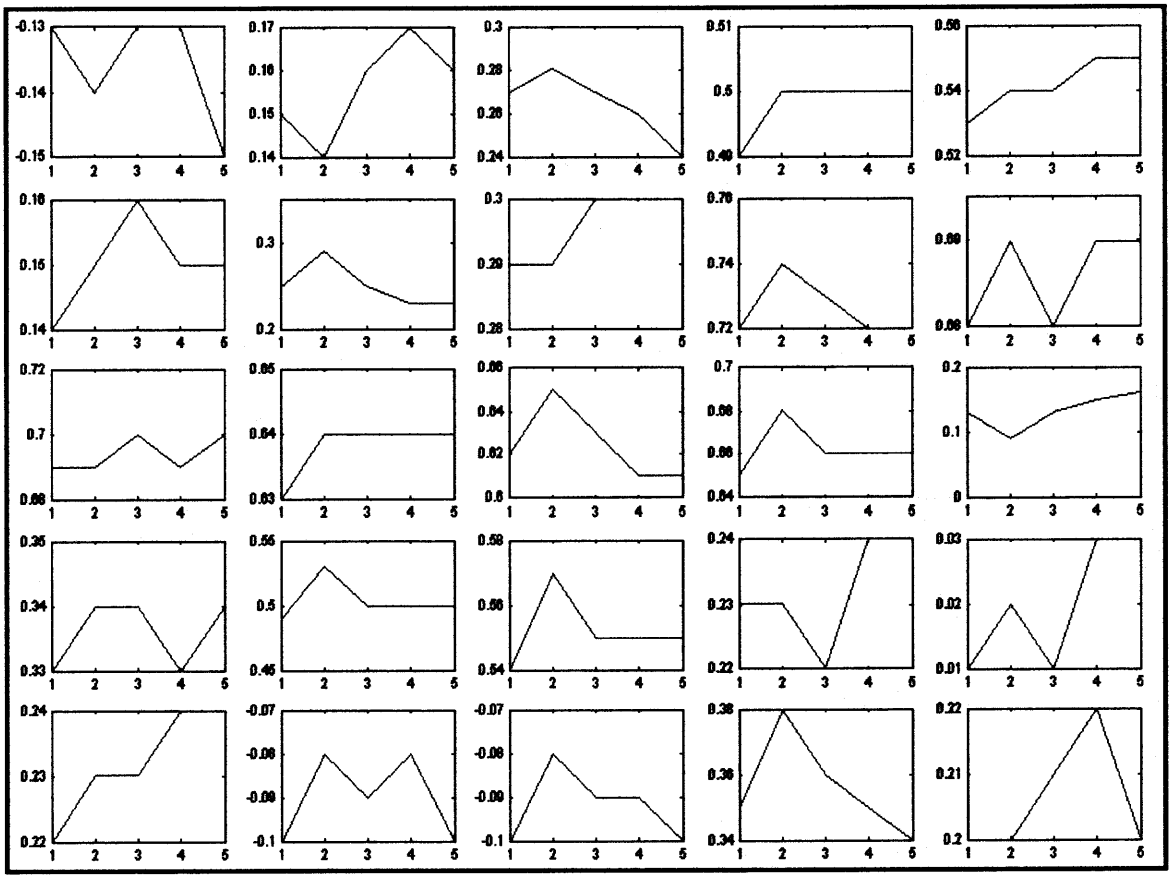

Figure 6.7 Represents subplots comparing mean correlation coefficient values obtained applying block bootstrap, with block sizes 34, 36, 38, 39 and 0 (conventional bootstrap resampling technique) for voxels in the motor cortex.

For this study the fMRI data were acquired for two different designs of task paradigm. For the first set of task paradigms, the 20 secs ON and OFF time period were used for TR = 2000 ms , TR = 1000 ms , TR = 500ms and TR = 250 ms. For the second set of task paradigm, 40 secs, 20 secs, 10 secs and 5 secs ON and OFF time periods were used for TR = 2000 ms , TR = 1000 ms, TR = 500 ms, TR = 250 ms, respectively.

The block size obtained for each TR, at which high mean correlation coefficient value was observed, for the first set of data is shown in Table 6.2 (a) and for the second set of data is shown in Table 6.2 (b).

Table 6.2 (a) Shows the Block Size Obtained for Each TR, for the First Dataset at Which Maximum Correlation Coefficient Values was Obtained

Subject 1				
TR(Time of repetition, ms)	2000	1000	500	250
Block Size	11	18	36	74
Subject 2				
TR	2000	1000	500	250
Block Size	12	24	36	82
Subject 3				
TR	2000	1000	500	250
Block Size	12	20	40	80
Subject 4				
TR	2000	1000	500	250
Block Size	11	18	36	79
Subject 5				
TR	2000	1000	500	250
Block Size	11	18	36	78
Subject 6				
TR	2000	1000	500	250
Block Size	11	18	39	80

Table 6.2 (b) Shows the Block Size Obtained for Each TR, for the Second Dataset at Which Maximum Correlation Coefficient Values was Obtained

Subject 1				
TR (Time of repetition, ms)	2000	1000	500	250
Block Size	22	18	18	No activation
Subject 2				
TR	2000	1000	500	250
Block Size	22	24	18	No activation
Subject 3				
TR	2000	1000	500	250
Block Size	20	20	18	No activation
Subject 4				
TR	2000	1000	500	250
Block Size	20	18	20	No activation
Subject 5				
TR	2000	1000	500	250
Block Size	22	18	18	No activation
Subject 6				
TR	2000	1000	500	250
Block Size	24	18	No activation	No activation

In the second set of data, for TR = 250 ms, since the ON (active) and OFF (rest) period was only for 5 secs, activation was not very evident. The ON and OFF time period was too short to obtain a good response from the brain to the stimulus.

Once the block size for each TR was determined, the activation maps were generated using a confidence interval of mean correlation coefficient greater than 8 times its standard deviation. To analyze the activation maps, two cases are examined – first for images with TR = 500 ms and second with TR = 1000 ms. The activation map generated using the bootstrap, block bootstrap resampling for the block size 36 and using a fixed threshold of 0.4 for the correlation coefficient, for the fMRI image acquired using TR = 500 ms is shown in Figure 6.8 (a), (b), (c), respectively.

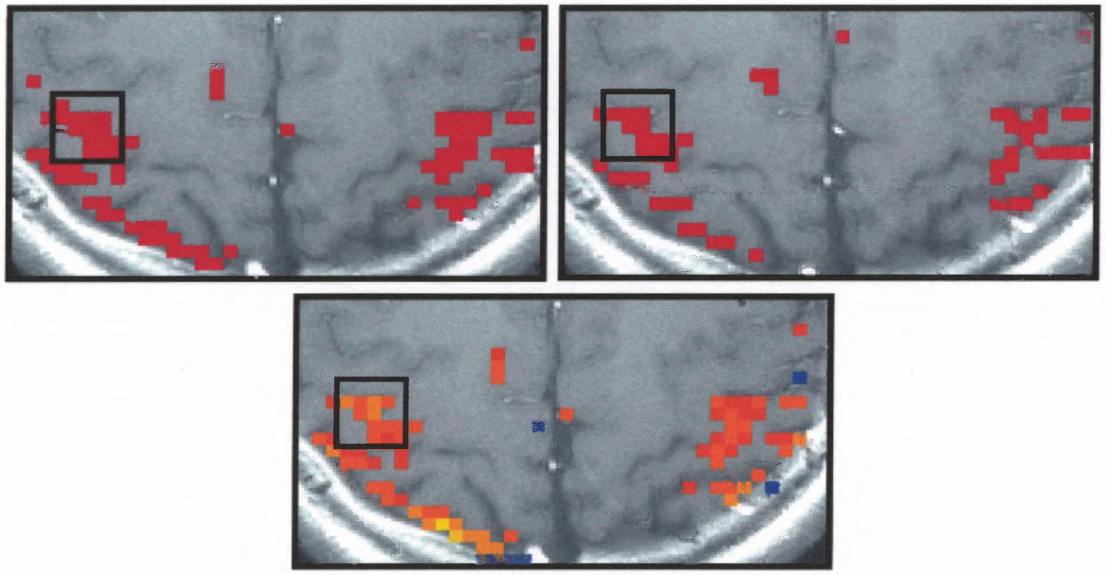

Figure 6.8 (a) (top left), (b) (top right), (c) (bottom) Shows the activation map that have same confidence internal at each voxel generated using the bootstrap resampling technique, block bootstrap resampling technique (block size 36) and using a fixed correlation coefficient threshold of 0.4 in AFNI, for the fMRI image acquired using TR = 500 ms.

Analyzing the activation maps shown in Figure 6.8, it can be noted that the number of active voxels detected varied for different techniques. It is evident that the activation map generated using the block bootstrap (i.e. considering temporal dependency in the fMRI dataset) shows less number of active voxels, when compared to the activation map generated using the conventional bootstrap and the activation map generated using AFNI.

To further analyze the active regions detected using different techniques, the time series of the voxels represented in Figure 6.8, are shown in Figure 6.9. From Figure 6.8 and Figure 6.9 it can be seen that the activation map generated using the block bootstrap shows only those voxels as active, whose signal time course show a good response to the stimulus reference waveform. The mean and standard deviation of the correlation coefficients generated using the bootstrap and block bootstrap for the voxels shown in Figure 6.8 is represented in Table 6.3 (a), (b). The histogram of the correlation coefficient values ranging from -1 to +1 generated using the bootstrap and block bootstrap resampling technique for the voxels shown in Figure 6.8 is represented in Figure 6.10 (a), (b).

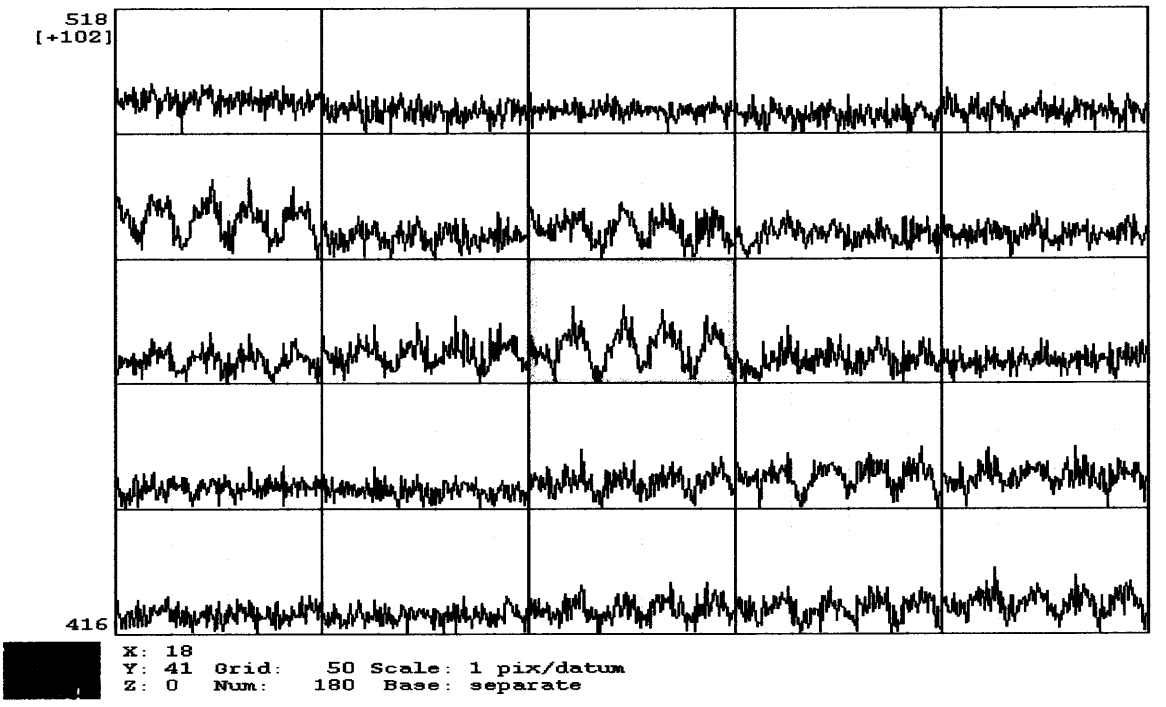

Figure 6.9 The time series of the fMRI image, which shows the response of the brain during bilateral finger tapping, acquired using TR = 500ms for the voxel shown in Figure 6.8.

Table 6.3 (a) Shows the Mean and Standard Deviation of the 1000 Correlation Coefficient Values Obtained Using the Bootstrap Resampling Technique for the Voxel Shown in Figure 6.8

0.37±0.04	-0.15±0.05	0.04±0.05	0.32±0.04	0.02±0.05
0.72±0.02	0.48±0.03	0.75±0.02	0.49±0.03	0.03±0.05
0.25±0.04	0.57±0.03	0.72±0.02	0.36±0.04	0.09±0.05
0.13±0.05	0.23±0.04	0.57±0.03	0.66±0.02	0.54±0.03
-0.09±0.05	0.18±0.05	0.49±0.03	0.41±0.03	0.54±0.03

Table 6.3 (b) Shows the Mean and Standard Deviation of the 1000 Correlation Coefficient Values Obtained Using the Block Bootstrap Resampling Technique for the Voxels Shown in Figure 6.8

0.41±0.06	-0.14±0.04	0.05±0.06	0.33±0.08	0.04±0.04
0.74±0.03	0.47±0.03	0.77±0.02	0.50±0.06	0.04±0.04
0.25±0.05	0.56±0.04	0.73±0.02	0.39±0.05	0.08±0.02
0.16±0.04	0.23±0.04	0.59±0.03	0.66±0.04	0.56±0.03
-0.1±0.07	0.20±0.05	0.48±0.03	0.41±0.04	0.55±0.03

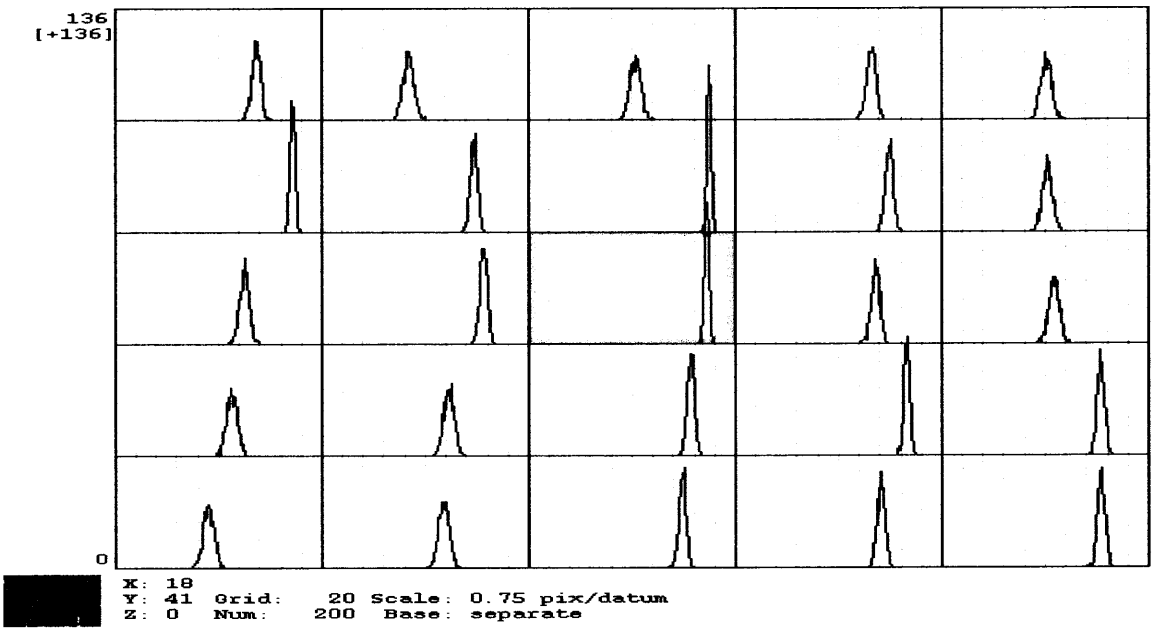

Figure 6.10 (a) Represents the histogram of the correlation coefficient values ranging from -1 to +1 obtained using the bootstrap resampling technique for the voxels shown in Figure 6.8.

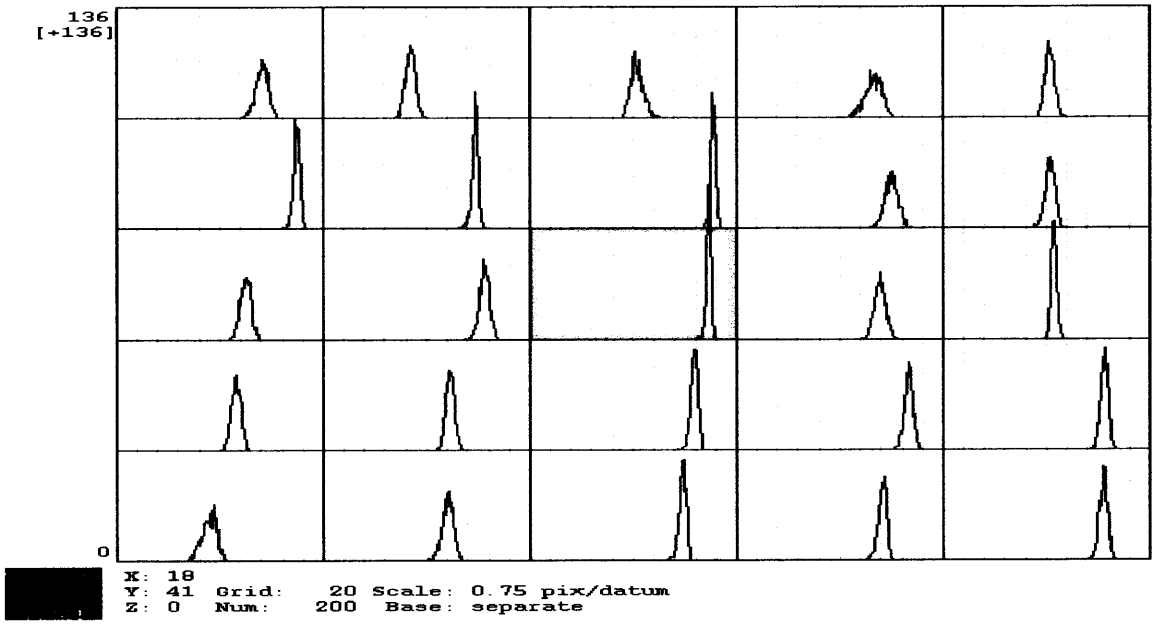

Figure 6.10 (b) Represents the histogram of the correlation coefficient values ranging from -1 to +1 obtained using the block bootstrap resampling technique for the voxels shown in Figure 6.8.

Figure 6.11 (a), (b) and (c) represents the activation maps for the fMRI image obtained using TR = 1000ms, generated using the bootstrap, block bootstrap resampling using a block size of 18 and fixed threshold of 0.4 for correlation coefficient value.

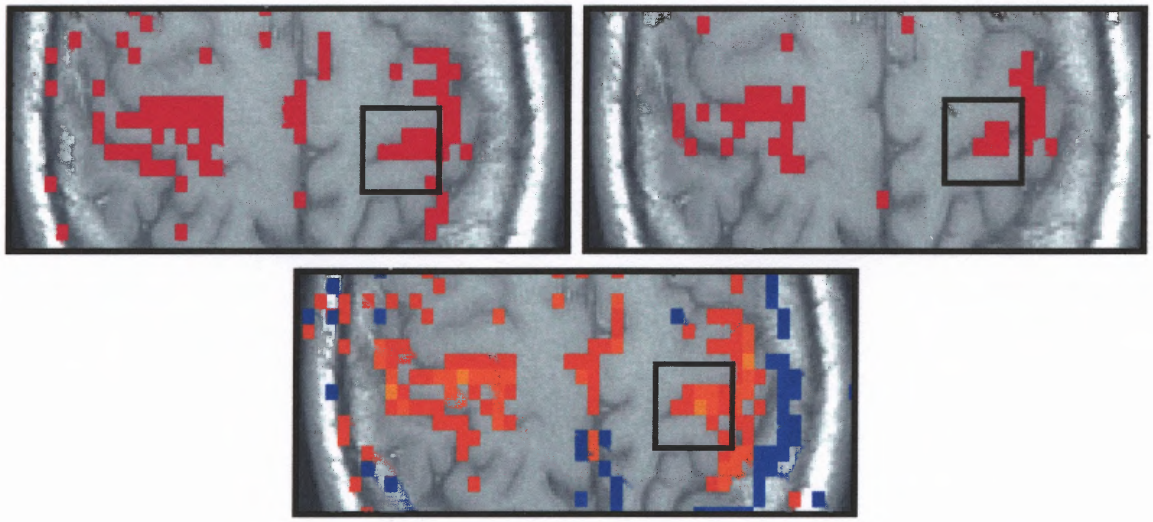

Figure 6.11 **(a)** (top left), **(b)** (top right), **(c)** (bottom) Shows the activation map that have same confidence internal at each voxel obtained using the bootstrap resampling technique, block bootstrap resampling technique (block size 18) and using a fixed correlation coefficient threshold of 0.4, for the fMRI image acquired using TR = 1000 ms.

Even for this case, it can be observed that the number of voxels shown as active differs for different techniques used. The time series for the voxels represented in Figure 6.11 is shown in Figure 6.12. The mean and standard deviation of the correlation coefficient values generated using the bootstrap and block bootstrap technique is shown in Table 6.4 (a) and (b) and their histogram with values ranging from -1 to +1 is shown in Figure 6.13 (a) and (b).

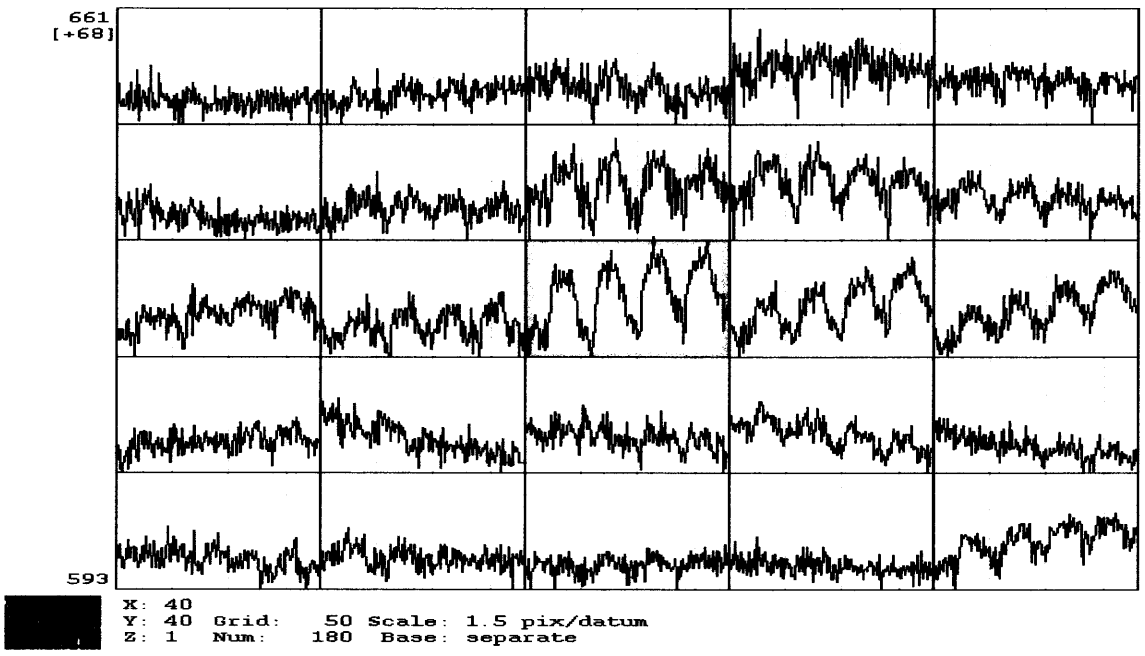

Figure 6.12 Represents the time series of the fMRI image, which shows the response of the brain during bilateral finger tapping, obtained using TR = 1000ms for the voxel shown in Figure 6.11.

Table 6.4 (a) Shows the Mean and Standard Deviation of the 1000 Correlation Coefficient Values Obtained Using the Bootstrap Resampling Technique for the Voxel Shown in Figure 6.11

-0.05±0.07	0.23±0.07	0.29±0.06	0.30±06	0.35±0.05
0.08±0.07	0.45±0.05	0.60±0.04	0.61±04	0.52±0.04
0.45±0.05	0.58±0.04	0.78±0.02	0.67±03	0.55±0.04
0.30±0.06	-0.19±0.06	0.26±0.06	0.39±05	0.11±0.07
0.09±0.07	0.23±0.07	0.27±0.07	0.07±07	0.56±0.04

Table 6.4 (b) Shows the Mean and Standard Deviation of the 1000 Correlation Coefficient Values Obtained Using the Block Bootstrap Resampling Technique for the Voxel Shown in Figure 6.11

-0.02±0.07	0.31±0.08	0.28±0.12	0.30±05	0.34±0.07
0.04±0.11	0.43±0.05	0.63±0.03	0.59±04	0.49±0.07
0.48±0.11	0.59±0.05	0.80±0.03	0.72±06	0.62±0.09
0.29±0.12	-0.30±0.15	0.19±0.11	0.33±16	0.04±0.19
0.01±0.13	0.22±0.09	0.32±0.06	0.05±0.09	0.61±0.08

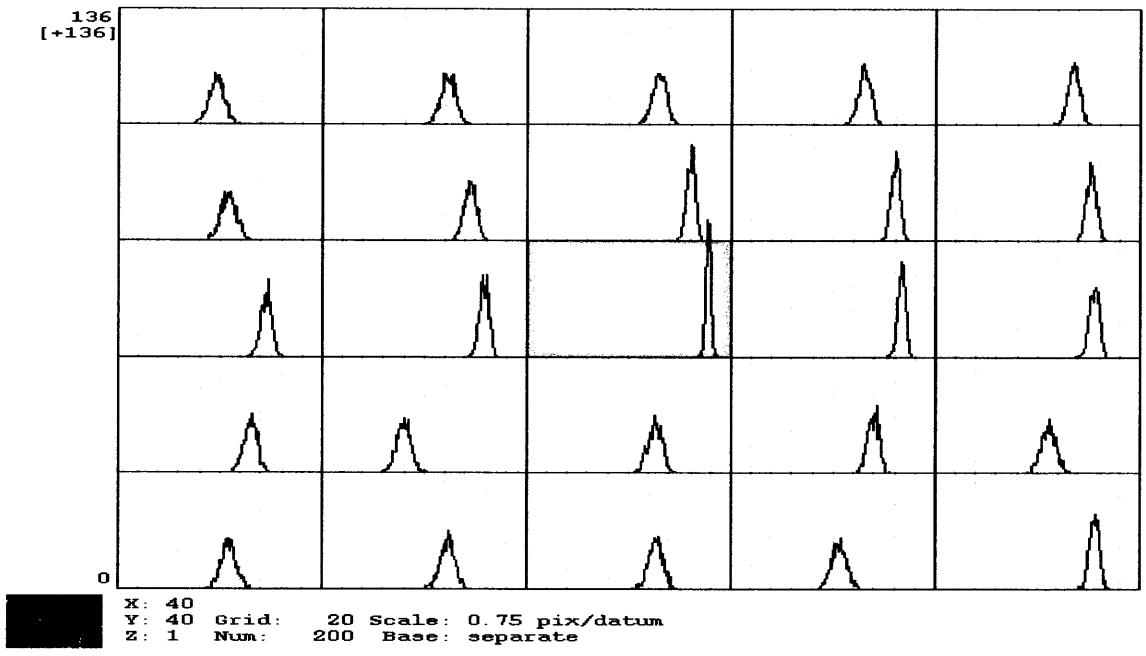

Figure 6.13 (a) Represents the histogram of the correlation coefficient values ranging from -1 to +1, obtained using the bootstrap resampling technique, for the voxels shown in Figure 6.11.

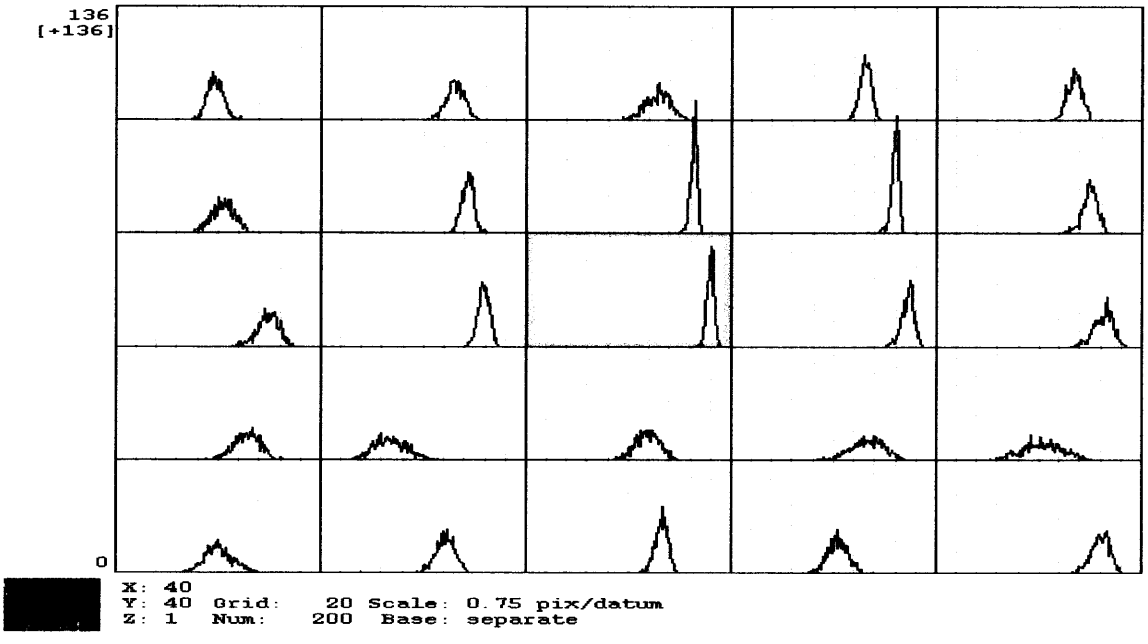

Figure 6.13 (b) Represents the histogram of the correlation coefficient values ranging from -1 to +1, obtained using the block bootstrap resampling technique, for the voxels shown in Figure 6.11.

Analyzing the activation maps generated using the conventional bootstrap, block bootstrap resampling technique and cross correlation technique, showed difference in the number and regions of active voxels. Table 6.5 (a) shows the difference in the number of voxels that were shown as active for the first dataset and Table 6.5 (b) shows the difference in the number of voxels that were shown as active for the second dataset using different techniques for the fMRI images obtained using different TR.

In the second set of data, for TR = 250 ms, since the ON (active) and OFF (rest) period was only for 5 secs activation was not very evident. The ON and OFF time period was too short to obtain a good response from the brain to the stimulus.

Analyzing Table 6.5 (a) and (b), it can be inferred that using the distribution of the correlation coefficients generated using the bootstrap resampling technique to detect active voxels show less number of voxels, when compared to using the fixed threshold method. Moreover, it can also be observed that by applying the block bootstrap resampling technique, even less number of active voxels are detected compared to the conventional bootstrap.

Table 6.5 (a) Represents the Number of Voxels that were Shown as Active Using Fixed threshold of correlation coefficient, Bootstrap Resampling Technique and Block Bootstrap Resampling Technique for the First Set of Data

TR (Time of repetition, ms)	Cross Correlation	Bootstrap Resampling Technique using Cross Correlation	Block Bootstrap Resampling Technique using Cross Correlation
Subject 1			
2000	83	41	42
1000	52	42	30
500	49	69	46
250	22	55	18
Subject 2			
2000	57	30	27
1000	47	40	27
500	32	48	25
250	24	43	14
Subject 3			
2000	50	25	18
1000	41	37	17
500	32	36	21
250	18	32	14
Subject 4			
2000	41	23	17
1000	63	43	30
500	28	36	25
250	16	41	8
Subject 5			
2000	55	31	41
1000	37	34	25
500	14	24	14
250	12	16	10
Subject 6			
2000	50	31	32
1000	40	30	18
500	21	22	21
250	7	16	9

Table 6.5 (b) Represents the Number of Voxels that were Shown as Active Using Fixed threshold of correlation coefficient, Bootstrap Resampling Technique and Block Bootstrap Resampling Technique for the Second Set of Data

TR (Time of repetition, ms)	Cross Correlation	Bootstrap Resampling Technique using Cross Correlation	Block Bootstrap Resampling Technique using Cross Correlation
Subject 1			
2000	91	25	18
1000	52	42	30
500	16	5	5
250	No activation	No activation	No activation
Subject 2			
2000	35	23	15
1000	47	40	27
500	11	5	1
250	No activation	No activation	No activation
Subject 3			
2000	56	34	11
1000	41	37	17
500	20	17	7
250	No activation	No activation	No activation
Subject 4			
2000	61	48	24
1000	63	43	30
500	36	23	3
250	No activation	No activation	No activation
Subject 5			
2000	44	38	32
1000	37	34	25
500	11	4	2
250	No activation	No activation	No activation
Subject 6			
2000	23	15	9
1000	40	30	18
500	4	No activation	No activation
250	No activation	No activation	No activation

6.5 Results Obtained Applying T-test

In order to check if a similar distribution of the voxels can be obtained by using methods other than cross correlation, t-values were calculated for the bootstrapped and block bootstrapped resampled data set. For applying the t-test, the average signal intensity during rest was subtracted from the average signal intensity during activation. If the t-values obtained by subtracting the signal intensities were high, then the voxel was considered to be active.

The activation maps for cross correlation and t-test using bootstrap and block bootstrap technique were generated using a confidence interval of mean greater than 8 times that standard deviation. Figure 6.14 (a) and (b) shows the activation map obtained by calculating the cross correlation and t-values for bootstrapped resampled data (without considering temporal dependency) for an fMRI image acquired using TR = 500 ms. Figure 6.15 (a) and (b) represents the histogram of the correlation coefficients ranging from -0.06 to 0.8 and t-values ranging from -0.6 to 12 obtained using the bootstrap resampling technique.

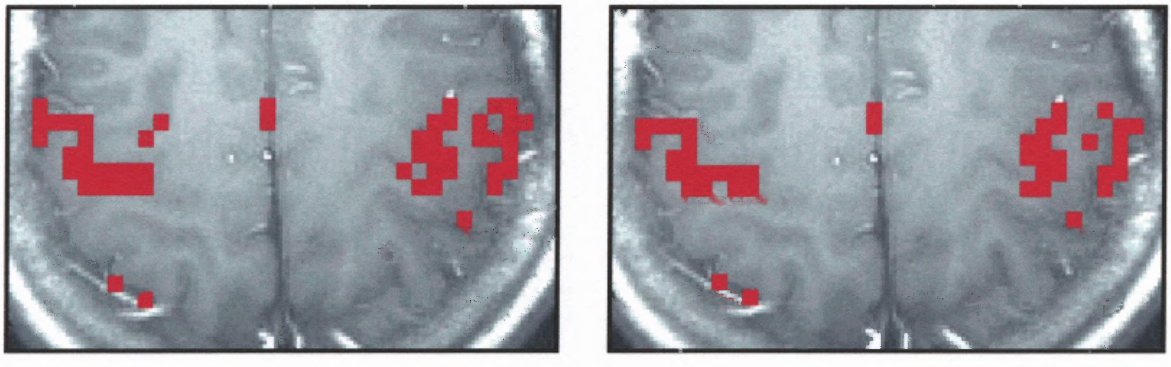

Figure 6.14 **(a)** (left), **(b)** (right) Shows the activation map that have same confidence internal at each voxel obtained using cross correlation and t-test for bootstrap resampled data set for the fMRI image acquired using TR = 500 ms.

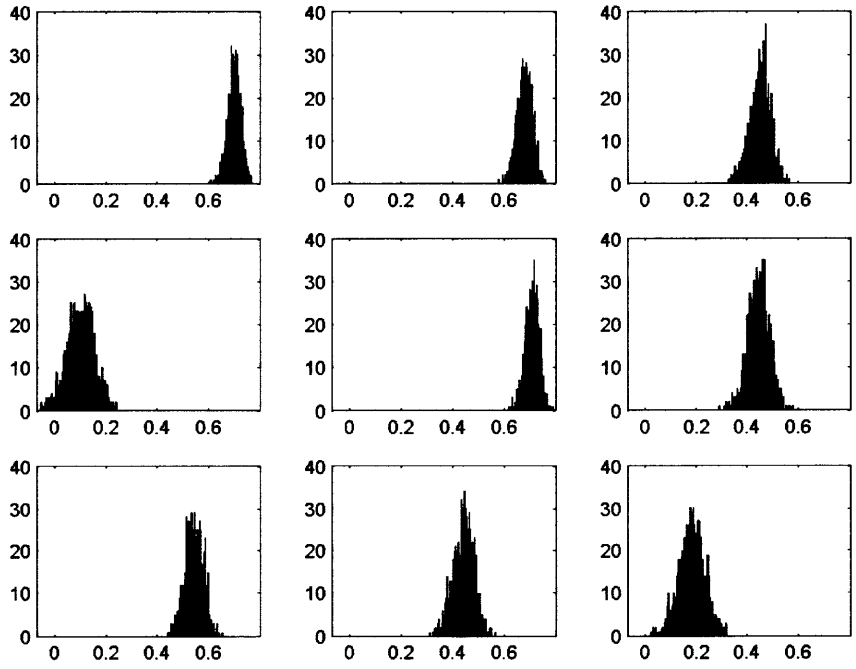

Figure 6.15 (a) Represents the histogram of the correlation coefficient values ranging from -0.06 to 0.8 obtained using the bootstrap resampling technique for the voxels shown in Figure 6.14 (a).

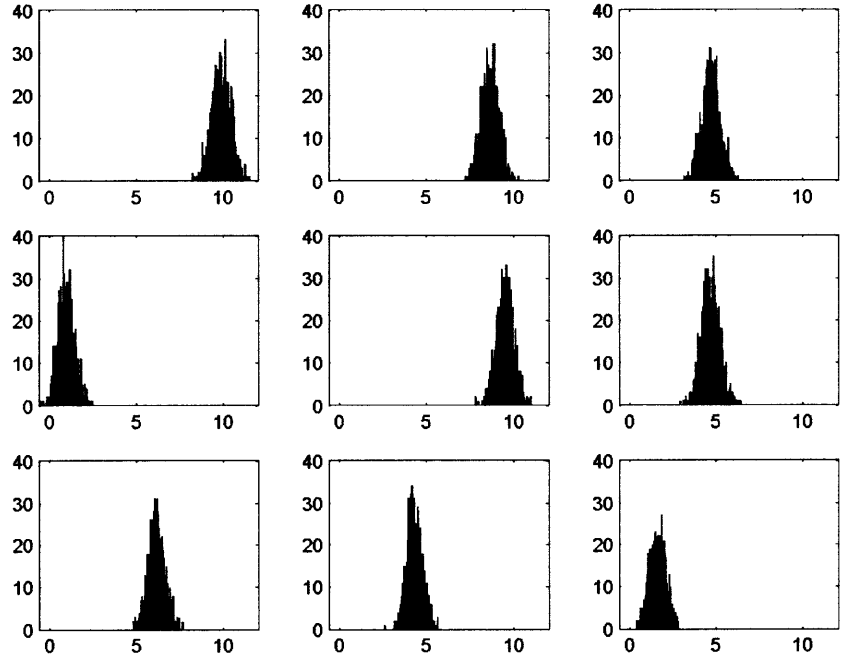

Figure 6.15 (b) Represents the histogram of the t-values ranging from -0.6 to 12 obtained using the bootstrap resampling technique for the voxels shown in Figure 6.14 (b).

Figure 6.16 (a) and (b) shows the activation map for an fMRI image acquired with TR = 500 ms, obtained by calculating the cross correlation and t-values for block bootstrapped data (considering temporal dependency). Figure 6.17 (a) and (b) represents the histogram of the correlation coefficients ranging from -0.2 to 0.8 and t-values ranging from -2 to 12 obtained using the block bootstrap resampling technique.

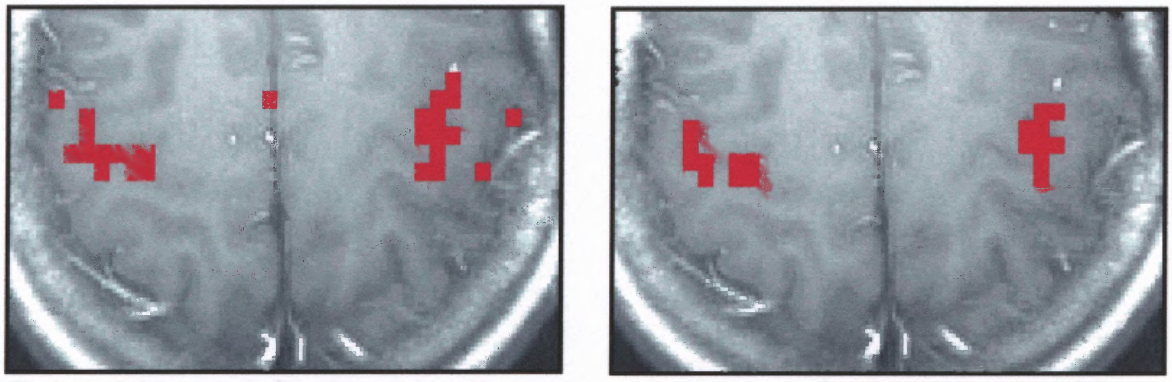

Figure 6.16 (a) (left), (b) (right) Shows the activation map that have same confidence internal at each voxel obtained using cross correlation and t-test for block bootstrap resampled data set (block size 36) for the fMRI image acquired using TR = 500 ms.

It can be inferred from Figures 6.14 (a) and (b) that the activation maps generated from cross correlation and t-values in the bootstrap resampling technique showed slight difference in the detection of active voxels. Also, observing the Figures 6.16 (a) and (b), the differences in the activation maps, generated from cross correlation and t-values in the block bootstrap resampling technique are evident.

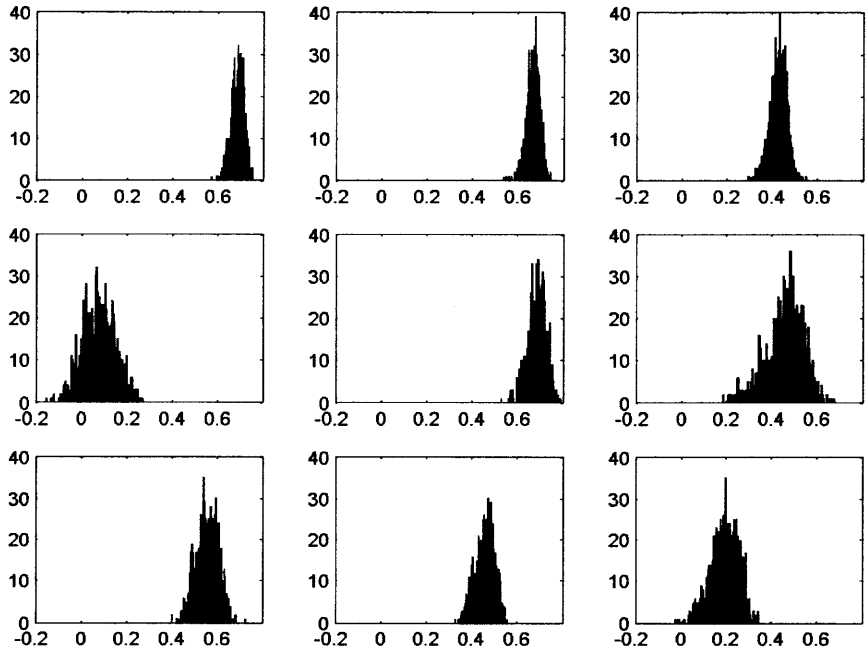

Figure 6.17 (a) Represents the histogram of the correlation coefficient values ranging from -0.2 to 0.8 obtained using the block bootstrap resampling technique for the voxels shown in Figure 6.16 (a).

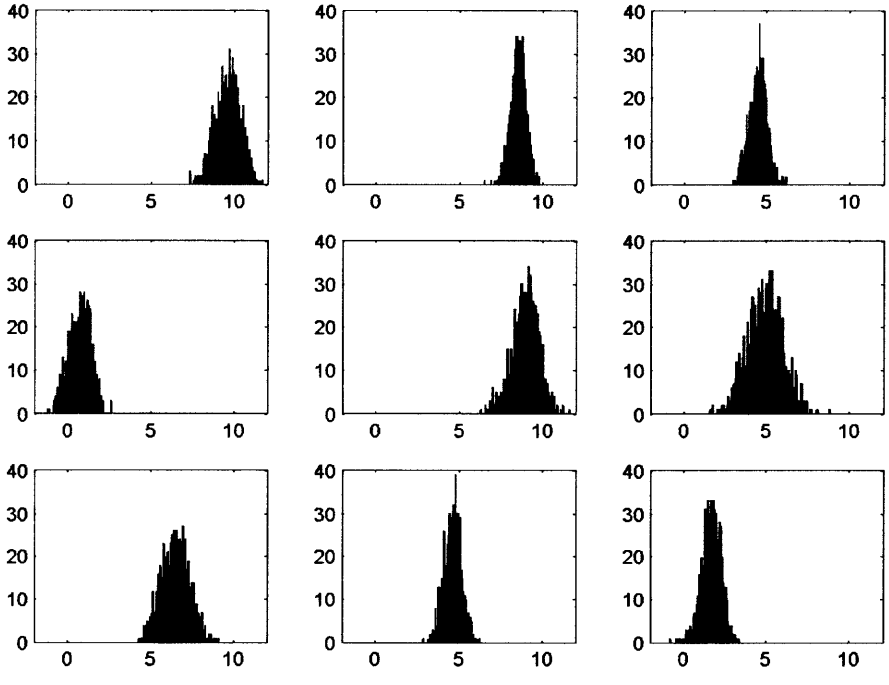

Figure 6.17 (b) Represents the histogram of the t-test values ranging from -2 to 12 obtained using the block bootstrap resampling technique for the voxels shown in Figure 6.16 (b).

Table 6.6 (a) compares the variation in the number of active voxels for the first dataset, detected using fixed threshold of t-values, bootstrap and block bootstrap technique using t-test and Table 6.6 (b) shows the same for the second dataset.

Table 6.6 (a) Represents the Number of Voxels that were Shown as Active Using Fixed Threshold of t-values, Bootstrap Resampling Technique Using T-test and Block Bootstrap Resampling Technique Using T-test for the First Set of Data

Subject 1			
TR (Time of repetition, ms)	**T-Test**	**Bootstrap Resampling Technique using t-test**	**Block Bootstrap Resampling Technique using t-test**
Subject 1			
2000	56	18	29
1000	15	26	19
500	30	62	33
250	35	46	14
Subject 2			
2000	45	17	13
1000	20	32	17
500	36	40	18
250	59	41	7
Subject 3			
2000	88	22	18
1000	44	36	26
500	44	36	12
250	28	12	9
Subject 4			
2000	62	10	10
1000	52	34	13
500	37	29	11
250	23	36	4
Subject 5			
2000	51	23	29
1000	39	24	17
500	83	16	11
250	4	13	7
Subject 6			
2000	85	17	18
1000	31	22	15
500	32	21	19
250	20	14	9

Table 6.6 (b) Represents the Number of Voxels that were Shown as Active Using Fixed Threshold of T-values, Bootstrap Resampling Technique Using T-test and Block Bootstrap Resampling Technique Using T-test for the Second Set of Data

TR (Time of repetition, ms)	Fixed Threshold of t-values	Bootstrap Resampling Technique using t-test	Block Bootstrap Resampling Technique using t-test
Subject 1			
2000	63	50	42
1000	15	26	19
500	1	2	1
250	33	No activation	No activation
Subject 2			
2000	13	17	9
1000	20	32	17
500	42	No activation	No activation
250	51	No activation	No activation
Subject 3			
2000	96	23	13
1000	44	36	26
500	24	No activation	No activation
250	4	No activation	No activation
Subject 4			
2000	64	42	10
1000	52	34	13
500	12	No activation	No activation
250	18	No activation	No activation
Subject 5			
2000	31	35	22
1000	39	24	17
500	30	No activation	No activation
250	34	No activation	No activation
Subject 6			
2000	99	11	6
1000	31	22	15
500	66	No activation	No activation
250	12	No activation	No activation

In the second data set, for TR = 250 ms and TR = 500 ms no activation was observed. This was due to poor signal response, which failed to show difference in the average signal intensity during rest and activation.

From Table 6.6 (a) and (b) it can be observed that using the block bootstrap resampling technique, less number of extraneous voxels was shown as active, when compared to the bootstrap resampling technique and fixed threshold of t-values.

6.6 Discussion

Analysis of the mean correlation coefficient values obtained using the block bootstrap showed higher correlation coefficient values when compared to those obtained from conventional bootstrap resampling technique. Observing the block size obtained for each TR (at which higher mean correlation coefficient values were obtained), shown in Table 6.2 (a) and (b), the presence of temporal dependency in the fMRI dataset is evident.

Analyzing Table 6.5 (a) and (b), it can be observed that the activation map generated using the conventional bootstrap resampling showed less number of active voxels, when compared to the activation map obtained using the fixed threshold of the correlation coefficient. It was also seen that, compared to the conventional bootstrap resampling, block bootstrap showed lesser number of active voxels. Analyzing the time series of the active voxels detected showed that using the block bootstrap, only those voxels were shown as active for which the time series has a good response to the stimulus waveform. Hence, using the block bootstrap resampling technique, considering temporal dependency in the fMRI data, better reliability of detecting active voxels can be achieved.

The results of the t-test showed slight variation in activation map compared to the activation map generated using the cross correlation in the bootstrap and block resampling technique. The difference in the methodologies of t-test and cross correlation can result in different distributions of the statistical parameter, which leads to variation in activation detections.

CHAPTER 7

CONCLUSION

Functional Magnetic Resonance Imaging is a noninvasive technique to detect regional changes in cerebral metabolism, blood flow volume or oxygenation in response to task activation. The critical step in functional MR imaging is the statistical analysis of the images. Prior to statistical analysis, the images need to be preprocessed, for motion correction and filtering, to reduce the noise and increase signal to noise ratio.

The most commonly used methods for statistical analysis are the linear parametric methods like t-test, cross correlation, and the general linear model. These methods use a fixed threshold of statistical parameter (t-test, f-test and cross correlation) to detect the active voxels. By using a fixed threshold, all voxels are assumed to be influenced by the same level of noise, which can lead to less reliable detection of active voxels.

To reliably detect active regions, researchers have used test-retest method. In the test-retest method the experiment is repeated multiple times using the same imaging parameters. The data obtained from multiple repetitions of the experiment is statistically analyzed. The test-retest methodology assumes that images are acquired under identical conditions for multiple repetitions of the experiment. This assumption may hold true for a simple motor or visual task, but for more complex tasks, this assumption will not be valid. For example, in a simple finger tapping experiment, the imaging parameters and the stimulus related parameters, like the finger tapping rate and the ON/OFF cycle timing, must be identical for each scan. Any deviation from the specified finger tapping rate, or the ON/OFF cycles in any of the scans, would result in erroneous detection.

Moreover, the reproducibility of fMRI data for each repetitive scan can be affected by attentional efforts, motion artifacts, repositioning errors, learning, habituation or fatigue. Further, for a number of cases involving children and trauma patients, it is not possible to repeat the study a number of times.

To overcome the limitations of conventional methods, resampling techniques like the jackknife and bootstrap have been developed to reliably detect the active regions. Using resampling techniques, it is possible to generate a large pseudo population of data, by repeatedly resampling from the original dataset. Hence, the necessity to repeat an experiment multiples times in order to obtain large amount of dataset can be avoided.

This study used the bootstrap resampling technique to estimate the reliability and confidence interval of correlation coefficients for fMRI image. Using the bootstrap resampling technique, the confidence interval of the correlation coefficients was determined by analyzing its distribution for each voxel. This resulted in generating activation maps that had the same confidence intervals at each voxel. Also, the different noise levels present at each voxel is taken into account while generating the activation map, unlike in hard thresholding where same noise levels are assumed among all voxels.

The Bootstrap resampling technique assumes that the fMRI dataset is independent and identically distributed over time. Studies on fMRI images acquired from the resting brain have shown fluctuations that are correlated with heart rate and respiratory rate and other fluctuations that are slower than cardiac or respiratory rate. This study investigated if higher reliability and confidence interval in detecting active regions can be achieved using the block bootstrap resampling technique, considering temporal dependency in the fMRI data.

Analysis of the results revealed that, considering temporal dependency in the data while applying the bootstrap resampling technique showed active voxels that has more reliability than those obtained without considering any temporal dependency in the data. Higher correlation coefficient values were observed using the block bootstrap when compared to the conventional bootstrap resampling. Analyzing the time series of the images showed that using the block bootstrap, only those voxels were shown as active whose signal time course has a good response to the stimulus reference waveform. Comparing the activation maps generated using the block bootstrap resampling technique, bootstrap resampling technique and fixed threshold of correlation coefficients, showed that activations detected using block bootstrap resampling technique were more localized and showed less extraneous active voxels compared to the other two methods.

Functional magnetic resonance imaging is being increasingly used to map the brain for surgical planning and for such high stake applications; it is essential to detect functional regions with high reliability. Hence, the use of statistical methods like bootstrap resampling technique is necessary.

In this study, cross correlation and t-test were used to generate confidence interval, other statistical parameters like F-test, ANOVA can also be used in the bootstrap resampling technique. In conclusion, applying the block bootstrap resampling technique incorporating the temporal dependency in the data can be used to determine the reliability and confidence interval of the statistical parameters. The active regions detected using this technique, was more reliable than the active regions detected by applying the conventional bootstrap resampling technique, without considering any temporal dependency in the data.

REFERENCES

[1] J. L. Marchini, B. D. Ripley. "A New Statistical Approach to Detecting Significant Activation in Funtional MRI". *NeuroImage*, vol. 12, pp. 366-380, 2000.

[2] B. A. Ardekani, I. Kanno. "Statistical Methods for Detecting Activated Regions in Functional MRI of the Brain". *Journal of Magnetic Resonance Imaging*, vol. 16, pp. 1217-1225, 1998.

[3] F. Z. Yetkin, T. L. McAuliffe, R. Cox, and V. M. Haughton. "Test-Retest Precision of Functional MR in Sensory and Motor Task Activation". *American Journal of Neuroradiology*, vol. 17, pp. 95-98,1996.

[4] S. A. Rombouts, F. Barkhof, F. G. Hoogenraad, M. Sprenger, J. Valk, and P. Scheltens. "Test-Retest Analysis with Functional MR of the Activated Area in the Human Visual Cortex". *American Journal of Neuroradiology*, vol. 18, pp. 1317-1322, 1997.

[5] C. R. Genovese, D. C. Noll, and W. F. Eddy. "Estimating Test-Retest Reliability in Functional MR Imaging. I: Statistical Methodology". *Journal of Magnetic Resonance in Medicine,* vol. 38, pp. 497-507, 1997.

[6] R. Maitra, S. R. Roys, and R. P. Gullapalli. "Test-Retest Reliability Estimation of Functional MRI Data". *Journal of Magnetic Resonance in Medicine*, vol. 48, pp. 62-70, 2002.

[7] D. C. Noll, C. R. Genovese, L. Nystrom, A. L. Vazquez, S. D. Forman, W. F. Eddy, and J. D. Cohen,. "Estimating Test-Retest Reliability in Functional MR Imaging. II: Application to Motor and Cognitive Activation Studies". *Journal of Magnetic Resonance in Medicine,* vol. 38, pp. 508-17, 1997.

[8] S. A. Rombouts, F. Barkhof, F. G. Hoogenraad, M. Sprenger, and P. Scheltens. "Within-Subject Reproducibility of Visual Activation Patterns with Functional Magnetic Resonance Imaging using Multislice Echo Planar Imaging". *Journal of Magnetic Resonance in Medicine*, vol. 16, pp. 105-113, 1998.

[9] W. C. M. Machielsen, S. A. Rombouts, F. Barkhof, P. Scheltens, P. M. P. Witter. "fMRI of Visual Encoding: Reproducibility of Activation". *Human Brain Mapping,* vol. 9, pp. 156-164, 2000.

[10] B. B. Biswal, T. A. Paul, and U. L. John. "Use of Jacknife Resampling Technique to Estimate the Confidence Intervals of fMRI Parameters". *Journal of Computer Assisted Tomography*, vol. 25, pp. 113-120, 2001.

[11] B. B. Biswal, A. Bappal. "The Use of Bootstrap Resampling Technique to Determine the Confidence Interval for fMRI Parameters", *Submitted*, 2004.

[12] B. B. Biswal, F. Z. Yetkin, V. M. Haughton, J. S. Hyde. "Functional Connectivity in the Motor Cortex of Resting Human Brain Using Echo-Planar MRI". *Journal of Magnetic Resonance in Medicine*, vol. 34, pp. 537-541, 1995.

[13] B. B. Biswal, J. V. Kylen and J. S. Hyde. "Simultaneous Assessment of Flow and BOLD Signals in Resting-State Functional Connectivity Maps". *NMR in Biomedicine*, vol. 10, pp. 165-170, 1997.

[14] M. J. Lowe, B. J. Mock, and J. A. Sorenson. "Functional Connectivity in Single and Multislice Echoplanar Imaging Using Resting-State Fluctuations". *Journal of Neuroimage*, vol. 7, pp. 119-132, 1998.

[15] J. Xiong, L. M. Parsons, J. Gao, and P. T. Fox. "Interregional Connectivity to Primary Motor Cortex Revealed Using MRI Resting State Images". *Journal of Human Brain Mapping*, vol. 8, pp. 151-156, 1999.

[16] D. Cordes, V. M. Haugton, K. Arfanakis, G. J. Wendt, P. A. Turski, C. H. Moritz, M. A. Quigley, and M. E. Meyerand. "Mapping Functionally Related Regions of the Brain with Functional Connectivity MR Imaging". *American Journal or Neuroradiology* , vol. 21, pp. 1636-1644, 2000.

[17] D. Cordes, V. M. Haughton, J. D. Carew, K. Arfanakis, J. D. Carew, P. A. Turski, C. H. Moritz, M. A. Quigley, and M. E. Meyerand. "Frequencies Contributing to Functional Connectivity in the Cerebral Cortex in 'Resting –State' Data". *American Journal of Neuroradiology*, vol. 22, pp. 1326-1333, 2001.

[18] D. Cordes, V. M. Haughton, J. D. Carew, K. Arfanakis, K. Maravilla. "Hierarchical Clustering to Measure Connectivity in fMRI Resting-State Data". *Journal of Magnetic Resonance Imaging*, vol. 20, pp. 305-317, 2002.

[19] C. Carel, I. Loubinoux, F. Alary, K. Boulanouar, I. Berry, I. Rascol, P. Celsis, and F. Chollet. "Neural Substrate for the Effects of Passive Training on Sensorimotor Cortical Representation: A Study with fMRI in Healthy Subjects". *Journal of Cerebral Blood Flow and Metabolism*, vol. 20, pp. 478-484, 2000.

[20] I. Loubinoux, K. Boulanouar, J. P. Ranjeva, C. Carel, I. Berry, O. Rascol, P. Celsis, and F. Chollet. "Cerebral fMRI Activation Modulated by a Single Dose of the Monoamine Neurotransmission Enhancers Fluoxetine (Prozac(R)) and Fenozolone (Ordinator(R)) During Hand Sensorimotor Tasks". *Journal of Cerebral Blood Flow and Metabolism*, vol. 19, pp. 1365-1375, 1999.

[21] N. F. Ramsey, K. Tallent, P. V. Gelderen, J. A. Frank, C. T. Moonen, and D. R. Weinberger. "Reproducibility of Human 3D fMRI Brain Maps Acquired During a Motor Task". *Journal of Human Brain Mapping*, vol. 4, pp. 113-121, 1996.

[22] I. Loubinoux, C. Carel, F. Alary, K. Boulanouar, G. Viallard, C. Manelfe, O. Rascol, P. Celsis, and F. Chollet. "Within-Session and Between-Session Reproducibility of Cerebral Sensorimotor Activation: A Test-Retest Effect Evidenced With Functional Magnetic Resonance Imaging". *Journal of Cerebral Blood Flow and Metabolism*, vol. 21, no. 5, pp. 592-607, 2001.

[23] E. M. Purcell, H. C. Torrey, and R. V. Pound. "Resonance Absorption by Nuclear Magnetic Moments in a Solid". *Physical Review,* vol. 69, pp. 37-38,1946.

[24] F. Bloch, W. W. Hansen, and M. Packard. "Nuclear Induction". *Physical Review,* vol. 69, pp. 127,1946.

[25] P. C. Lauterbur, "Image Formation by Induced Local Interactions: Examples Employing Nuclear Magnetic Resonance". *Nature,* vol. 242, pp. 190-191, 1973.

[26] P. Mansfield, and P. K. Grannell. "NMR 'Diffraction' in Solids?". *Journal of Physics. Condensed Matter* , vol. 6, pp. L422-L426, 1973.

[27] J. P. Hornak. Basics of MRI.1996. Retrieved on March 30, 2004 from World Wide Web : http://www.cis.rit.edu/htbooks/mri/

[28] P. Mansfield. "Imaging by Nuclear Magnetic Resonance". *Journal of Physics E: Scientific Instruments*, vol. 21, pp. 18-30, 1988.

[29] J. T. Bushberg, J. A. Seibert, E. M. Leidholdt, J. M. Boone. "The Essential Physics of Medical Imaging". *Williams & Wilkins*, 2002.

[30] J. R. Ballinger. MRI Pulse Sequences. 1994. Retrieved on March 30, 2004 from World Wide Web : http://www.mritutor.org/mritutor/pulseseq.htm

[31] S. Ogawa, T. M. Lee, A. R. Kay, and D. W. Tank. "Brain Magnetic Resonance Imaging with Contrast dependent on Blood Oxygenation". *Proceedings of National Academy of Sciences,* vol. 87, pp. 9868-9872, 1990.

[32] D. C. Noll. "A Primer on MRI and Functional MRI". Retrieved on March 30, 2004 from World Wide Web: http://www.eecs.umich.edu/~dnoll/primer2.pdf

[33] A. M. Harner. "An Introduction to Functional Magnetic Resonance Imaging (FMRI) for Studying Visual Perception". Retrieved on March 30, 2004 from World Wide Web: http://people.bu.edu/harnera/papers/FMRI.pdf

[34] E. A. DeYoe, P. Bandettini, J. Neitz, D. Miller and P. Winans. "Functional magnetic Resonance Imaging (FMRI) of the human brain". *Journal of Neuroscience Methods,* vol. 54, no. 5 pp. 171-187. 1994.

[35] C. Stuart. "Functional Magnetic Resonance Imaging: Methods and Application". University of Nottingham. 1997.

[36] G. T. Buracas and G. M. Boynton."Efficient Design of Event-Related Fmri Experiments Using M-Sequences". *NeuroImage,* vol. 16, pp. 801-13, 2002.

[37] J. H. Gao, L. Miller, S. Lai, L. Xiong, P. T. Fox. "Quantitative Assessment of Blood Inflow Effects in Functional MRI Signals". *Journal of Magnetic Resonance Imaging*, vol. 36, pp. 314-319.

[38] C. R. Fisel, J. L. Ackerman, R. B. Buxton, L. Garrido, J. W. Belliveau, B. R. Rosen, and T. J. Brady. "MR Contrast Due to Microscopically Heterogeneous Magnetic Susceptibility: Numerical Simulations and Applications to Cerebral Physiology". *Journal of Magnetic Resonance in Medicine,* vol. 17, pp. 366-347,1991.

[39] J. Hykin, R. Bowtell, P. Mansfield, P. Glover, R. Coxon, R., B. Worthington, and L. Blumhardt. "Functional Brain Imaging Using EPI at 3T". *Magma,*vol. 2, pp. 347-349, 1994.

[40] B. Hamre. "The Three Dimensional Image Registration of Magnetic Resonance (MRI) Head Volumes". University of Bergen Norway. 1998.

[41] R. P. Woods, S. R. Cherry and J. C. Mazziotta. "Rapid Automated Algorithm for Aligning and Reslicing PET-Images". *Journal of Computer Assisted Tomography*, vol. 16, no. 4, pp. 620-633, 1992.

[42] A. Collignon, F. Maes, D. Delaere, D. Vandermuelen, P. Suetens, and G. Marchal. "Automated Multi-Modality Image Registration Based on Information Theory". *Proceedings in 14th International Conference of Information Processing in Medical Imaging (Breast*), pp. 263-274, 1995.

[43] P. A. Viola, W. M. Wells. "Alignment by Maximization of Mutual Information". *Proceedings 5th International Conference in Computer Vision*, pp. 16-23, 1995.

[44] J. V. Hajnal, N. Saeed, E. J. Soar, A. Oatridge, I. R. Young, and G. M. Bydder. "Registration and Interpolation Procedure for Subvoxel Matching of Serially Acquired MR Images". *Journal of Computer Assisted Tomography*, vol. 19, no. 2, pp. 289-296, 1995.

[45] P. A. Lynn. "An Introduction to the Analysis and Processing of Signals". *Macmillan*,1989.

[46] D. N. Plotis. "Computer-Intensive Methods in Statistical Analysis". *IEEE Signal Processing Magazine*, pp. 39-56,1998.

[47] A. M. Zoubir and B. Boadshash. "The Bootstrap and its Application in Signal Processing". *IEEE Signal Processing Magazine*, pp. 56-76, 1998.

[48] E. Bradley. "The Jackknife, the Bootstrap and Other Resampling Plans". *Cbms-Nsf Regional Conference Series in Applied Mathematics*, 1982.

[49] F. J. M. Bryan. "Randomization, Bootstrap and Monte Carlo Methods in Biology". *Chapman and Hall/CRC*, 1997.

[50] A. C. Davison, and D. V. Hinkley. "Bootstrap Methods and their Application". *Cambridge University Press*, 1999.